Study of charged-pseudoscalar-meson photoproduction from hydrogen and deuterium with 16-GeV linearly polarized photons

D. J. Quinn,* J. P. Rutherfoord,[†] and M. A. Shupe[‡]

Tufts University, Medford, Massachusetts 02155

D. J. Sherden, R. H. Siemann,[§] and C. K. Sinclair

Stanford Linear Accelerator Center, Stanford University, Stanford, California 94305

(Received 23 April 1979)

The asymmetries in forward π-N, π-Δ, and K^+-$(\Lambda + \Sigma)$ photoproduction have been measured with a 16-GeV linearly polarized beam. The experimental method and the procedures for extracting cross sections and asymmetries from the data are discussed in detail. Information on the energy and momentum-transfer dependence of cross sections for natural- and unnatural-parity exchange, interference between exchanges of opposite G parity, and vector-meson dominance is obtained and discussed.

I. INTRODUCTION

The study of pseudoscalar-meson photoproduction, although often included as a branch of lepton and photon physics, shares many concepts with purely hadronic-interaction studies. Through connections such as vector dominance the photon can be thought of as a strongly interacting particle. It is therefore not surprising to find similar theoretical interpretations for photoproduction and strong-interaction experiments.

There are, however, important differences which distinguish pseudoscalar-meson photoproduction from other strong-interaction processes. Since the photon has two possible spin states and does not have a unique isospin, more amplitudes are necessary to describe photoproduction, as opposed to production by pseudoscalar mesons, of any particular final state. This complication is compensated for by several advantages of photoproduction studies. For example, it is possible to study the photoproduction of all members of the pseudoscalar nonet, free of any diffractive channels, with a single beam. Furthermore, many reactions can be measured with a single experimental setup, providing a relatively systematic-error-free view of a large body of data.

A significant advantage of photoproduction is that with a linearly polarized photon beam one can obtain information on the naturality of t-channel exchanges. The asymmetry in pseudoscalar-meson photoproduction with linearly polarized photons is defined as

$$\Sigma(t) \equiv \frac{d\sigma_\perp/dt - d\sigma_\parallel/dt}{d\sigma_\perp/dt + d\sigma_\parallel/dt} , \tag{1}$$

where $d\sigma_\perp/dt$ ($d\sigma_\parallel/dt$) is the cross section for photons polarized perpendicular (parallel) to the production plane defined by the photon and detected

pseudoscalar meson. Using crossing-symmetry arguments Stichel[1] showed that to leading order in t/s, $d\sigma_\perp/dt$ ($d\sigma_\parallel/dt$) can receive contributions from only natural- (unnatural-) parity exchange in the t channel. Stichel obtained this result for single-pion photoproduction from nucleons; other authors[2] have extended this result to the general case of any allowed pseudoscalar-meson-plus-baryon final state.

In 1962 Cabbibo et al.[3] proposed using coherent pair production in crystalline material to polarize high-energy photon beams, and in 1970 Berger et al.[4] verified this polarization technique using compression-annealed pyrolytic graphite. Based on this work, we constructed a polarized photon beam which allowed significant new measurements of the asymmetry for many pseudoscalar photoproduction reactions. In this paper we present a detailed description of the experiment as well as the final results. These results are for three separate classes of reactions: single-pion photoproduction ($\gamma p \to \pi^+ n$ and $\gamma n \to \pi^- p$), π-Δ photoproduction ($\gamma p \to \pi^- \Delta^{++}$, $\gamma p \to \pi^+ \Delta^0$, $\gamma n \to \pi^- \Delta^+$, and $\gamma n \to \pi^+ \Delta^-$), and K^+ photoproduction ($\gamma p \to K^+ \Lambda$, $\gamma p \to K^+ \Sigma^0$, and $\gamma n \to K^+ \Sigma^-$). Brief summaries of our results, some of which have been published in previous papers,[5,6] and their relationship to previous experiments follow.

(i) *Single-pion photoproduction.* Before this experiment, the asymmetry for single-π^+ photoproduction had been measured up to 12-GeV incident energy.[7-10] These measurements showed that the asymmetry is essentially energy independent, and that this reaction is dominated by natural-parity exchange for $|t| > m_\pi^2$. Our results are in agreement with these earlier measurements.

The π^- asymmetry had been measured up to only 3.4-GeV incident energy.[11,12] At that energy there are significant contributions from unnatural-

parity exchange. Combining these lower-energy measurements with our data shows that the un-natural-parity-exchange cross section is energy dependent; this dependence is consistent with that expected from a simple pion Regge trajectory.

Our data and the lower-energy data for both π^+ and π^- photoproduction have several features in common. There is evidence for significant inter-ference between natural-parity exchanges of op-posite G parity, and no evidence for such inter-ference between unnatural-parity exchanges. The vector-dominance comparison between our mea-sured asymmetries and the density matrix ele-ments for $\pi^-p \to \rho^0 n$ shows poor agreement.

(*ii*) π-Δ *photoproduction*. Previous measure-ments of the asymmetries for these processes are limited,[10,13,14] and our measurements are the first with statistical significance. All four processes are dominated by natural-parity exchange at large $|t|$ and unnatural-parity exchange at small $|t|$.

Charge ratios for both perpendicular and parallel photons show significant interference between exchanges of opposite G parity. For perpendicular photons this interference is almost completely destructive at $t \simeq -0.15$ GeV^2 leading to a dip in the natural-parity exchange cross section for $\gamma p \to \pi^-\Delta^{++}$ and for the sum $\gamma p \to \pi^+\Delta^0$ plus $\gamma n \to \pi^+\Delta^-$ (measured from a deuterium target).

A vector-dominance comparison between our data and data from $\pi^+p \to \rho^0\Delta^{++}$ shows good agree-ment for the asymmetries and a similar t de-pendence for the cross sections.

(*iii*) K^+ *photoproduction*. These are the first measurements of the K^+ polarized-photon asym-metry. Because of the small difference between the Λ and Σ masses, the asymmetries for individ-ual processes are difficult to determine. Much greater confidence can be placed in the asym-metry for the sum of processes (e.g., for the sum $\gamma p \to K^+\Lambda$, $\gamma p \to K^+\Sigma^0$, and $\gamma n \to K^+\Sigma^-$ from a deuter-ium target). This combined asymmetry has been measured from both hydrogen and deuterium tar-gets, and for each target it rises from 0 at $t_{\min}$ to 1.0 for $|t| > 0.05$ GeV^2. Therefore, K^+ photopro-duction is dominated by natural-parity exchange.

We also present asymmetry results for individ-ual processes, and make some qualitative argu-ments about the nature of the s-channel helicity amplitudes for K^+ photoproduction.

II. EXPERIMENTAL DETAILS

A plan view of the experimental arrangement is shown in Fig. 1. A 16.05-GeV linearly polarized bremsstrahlung beam was incident on either a liquid-hydrogen or liquid-deuterium target. Photoproduced mesons were identified and mo-
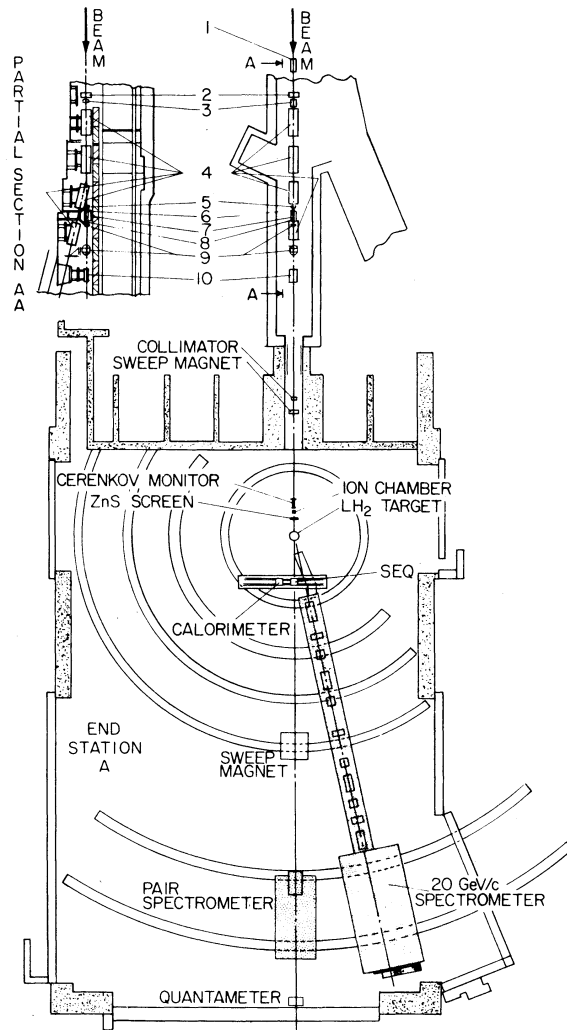

FIG. 1. Schematic of the photon beam line and experi-mental layout. The pair spectrometer was used during studies of the beam spectrum and polarization. The numbered elements in the beam line before the target are (1) toroid, (2) radiator, (3) Cherenkov position mon-itor, (4) electron beam dump magnets, (5) collimator, (6) graphite polarizer, (7) sweep magnet, (8) graphite analyzer (9) collimators, and (10) sweep magnet.

mentum-analyzed with the SLAC 20-GeV/c spec-trometer. Analysis of the pion or kaon momentum spectra permitted a separation of the various two-body reactions contributing to the total yield of these particles.

In the following sections, we describe the com-ponents of the experiment in some detail, indicate the sources of various uncertainties and correc-tions, and describe our data-taking procedures.

A. Polarized photon beam

A thorough description of the photon beam de-veloped for this experiment has been published.[15]

Only a summary of the beam production and its characteristics is presented here.

A 16.05-GeV electron beam from the Stanford Linear Accelerator passed through a beam-transport system containing ±0.25% energy-defining slits, struck a 0.0285-radiation-length aluminum radiator, and was then deflected into a beam dump. The unpolarized bremsstrahlung from the radiator passed through 61 cm of compression-annealed pyrolytic graphite, in which it was partially linearly polarized and unavoidably attenuated. The polarization mechanism was the preferential absorption, through coherent pair production, of one linear-polarization state from the unpolarized incident bremsstrahlung. The polarization plane was rotated by rotating the graphite about an axis along the beam.

The beam was collimated immediately before and after the polarizing graphite crystals, and at two other locations further downstream, before reaching the experimental target. Sweeping magnets were located after each of the latter two collimators, and the polarizing crystals were located in the field of a third sweeping magnet. With the collimation normally employed, the beam-spot size at the target was approximately 2 cm by 2 cm. The photon-beam position at the target was controlled by two small steering magnets upstream of the aluminum radiator. The electron-beam position at the radiator was monitored by a remotely viewed helium Cherenkov position monitor immediately downstream of the radiator, while the photon-beam position at the target could be observed remotely on removable zinc-sulphide screens upstream of the target. These screens were removed during data taking. The photon beam was dumped into a secondary-emission quantameter[16] located beyond the target.

The intensity of the initial bremsstrahlung beam was attenuated by a factor of about 20 in the polarizing crystal. The energy spectrum of the attenuated and polarized beam near the end-point energy was similar to that of ordinary bremsstrahlung. Thus we chose to relate the number of quanta of energy k to $k+dk$ in the final beam, $Cn(k)dk$, to the number in the initial bremsstrahlung beam, $C_0 n_0(k)dk$, by an attenuation function $A(k)$, such that

$$n(k) = A(k)n_0(k) .$$

Both $n(k)$ and $n_0(k)$ are normalized such that

$$\int_0^{E_0} kn(k)dk = \int_0^{E_0} kn_0(k)dk = E_0 ,$$

where E_0 is the bremsstrahlung end-point energy. C_0 and C thus represent the number of equivalent quanta in the initial and final beams. Typical
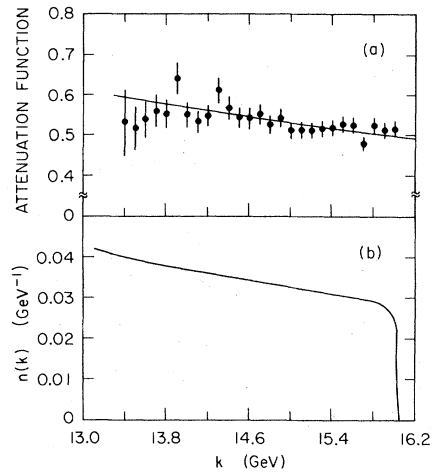

FIG. 2. (a) Measured attenuation function, $A(k)$, of the beam. The solid curve is a fit to the data. See Ref. 15 for details. (b) Photon-beam energy spectrum obtained by multiplying the bremsstrahlung spectrum for a 16.05-GeV electron beam times the fit to $A(k)$.

values in the present experiment were $C_0 = 4 \times 10^9$ and $C = 2 \times 10^8$ equivalent quanta per SLAC beam pulse.

The incident spectrum $n_0(k)$ was calculated to an accuracy of ±3% near E_0.[17] $A(k)$ was determined by comparing the incident and attenuated bremsstrahlung spectra, which were measured with the SLAC pair spectrometer.[18] The measurements of $A(k)$ in the region near E_0 are shown in Fig. 2(a). We have parametrized $A(k)$ as a linear function of k, as expected from the calculated properties of the crystal polarizer. The uncertainty in our one-parameter fit to $A(k)$ is estimated to be ±0.8%. In Fig. 2(b) we show $n(k)$.

While uncertainties in $A(k)$ and $n_0(k)$ affect the normalization of measured cross sections, they do not influence asymmetry measurements. Asymmetry measurements are affected only by differences in $A(k)$ between the two beam polarizations. We have determined $A(k)$ for both beam polarizations, and the results are consistent with $A(k)$ being polarization independent. We estimate the systematic uncertainty in our quoted asymmetries due to any polarization dependence of $A(k)$ to be less than ±0.025.

The polarization of the beam was measured to be 0.255 ± 0.020 for photon energies between 13.5 and 16 GeV by using a second graphite-crystal assembly 30.5 cm long to analyze the polarization produced by the first crystal. The uncertainty in the measured polarization introduces a systematic uncertainty into each asymmetry of ±8% of itself. Measurements of the asymmetry in $\gamma p \to \pi^+ n$ at $|t| = 0.15$ (GeV/c)^2, made several times during the course of the experiment, demonstrated that the

beam polarization remained constant to within
±0.008.

B. Beam-flux measurement

For all data but that obtained at the smallest
angle, the secondary-emission quantameter (SEQ)
served as our primary photon-beam monitor. The
beam was also monitored by a thin ion chamber
and a helium-filled Cherenkov monitor,[16] both lo-
cated upstream of the target. The electron beam
incident on the radiator was monitored by a pre-
cision toroid.[19] Yields from these various mon-
itors were intercompared at the end of each run
to check for beam-steering drifts, incorrect col-
limator settings, etc.

The measurements of $A(k)$ were done at very
low beam intensities to obtain reasonable counting
rates in the pair spectrometer. A gas-filled quan-
tameter[20] was used to monitor the beam for these
measurements. This point is important, since
the quantameter responds to the total beam energy
as does the SEQ used as the beam monitor for the
asymmetry measurements.

The SEQ response was compared to that of a
precision silver calorimeter[16] using the Cheren-
kov monitor as an intermediary. The SEQ re-
sponse varied by less than 1% with respect to that
of the silver calorimeter during the experiment,
and was independent of beam polarization to less
than 0.3%.

Both the ion chamber and the Cherenkov monitor
were found to have polarization-dependent respon-
ses when compared to the SEQ. For the Cheren-
kov monitor, this difference is typically less than
0.6% between the two polarizations. As the beam
spectrum was found to be polarization independent
when monitored with a total absorption device, we
attribute the polarization dependence observed in
the thin monitors to slight differences in the beam
halo, rather than to the SEQ. Both the ion cham-
ber and the Cherenkov monitor are much more
sensitive to beam halo than the SEQ.

For the data obtained at the smallest angle, 0.3°,
the SEQ could not remain in the beam as it would
have blocked the spectrometer aperture. For
these data, the Cherenkov monitor was used to
measure the beam flux. The polarization depen-
dence of the Cherenkov monitor was removed by
performing frequent SEQ–Cherenkov-monitor in-
tercomparisons for both polarizations. This pro-
cedure introduces an additional ±0.5% uncertainty
in both the cross section and asymmetry measure-
ments at this angle.

For data taken at 0.7°, it was necessary to move
the SEQ partially out of the beam. This resulted
in a different SEQ calibration and an additional
±0.6% uncertainty in the 0.7° cross sections. We

do not believe this procedure introduced additional
error into the asymmetry measurements at this
angle.

In determining the photon-beam flux, a correc-
tion was made for pair production in the material
in the beam after the last sweeping magnet. There
were 0.011 radiation lengths of material in addition
to the target; half the target length was used in
calculating its contribution to the correction. The
uncertainty in this correction adds an uncertainty
of ±0.5% to all cross sections and does not affect
the uncertainties in the asymmetry measurements.

C. Hydrogen and deuterium targets

1-meter-long condensation-type[21] liquid hydro-
gen and deuterium targets were used. These tar-
gets and a third identical dummy cell were ar-
ranged in a remotely driven vertical array. The
downstream end of the targets was horizontally
wider than the upstream end to ensure that all
detected particles left the target through the 0.10-
mm stainless-steel end windows.

The target cell lengths were measured warm and
a correction for the decrease in length with tem-
perature was calculated. The uncertainty in the
target length at liquid-hydrogen temperatures was
±0.1%. The target liquid was circulated with
pumps to ensure there were no gas bubbles in
the target. The target temperature was monitored
with hydrogen vapor pressure thermometers, and
was observed to be constant to ±0.5°K, corres-
ponding to density fluctuations of ±1%.

D. The SLAC 20-GeV/c spectrometer

The SLAC 20-GeV/c spectrometer,[22] shown in
Fig. 3, was used to detect particles photoproduced
in the target. The spectrometer contains four
dipoles, four quadrupoles, and three sextupoles,
mounted in a frame which can be remotely rotated
about the target center. The detectors are mounted
in a mechanically separate concrete shielding hut
which moves with the magnet frame.

1. Spectrometer optics

The first-order optical properties of the spec-
trometer are illustrated in Fig. 4. Information
on the measured optical properties is available in
the SLAC User's Handbook.[23] All trajectory mea-
surements for the present experiment were made
with scintillation counter hodoscopes in the detec-
tor hut.

In the horizontal plane, the spectrometer is
parallel-to-point focusing, causing particles of
the same horizontal production angle to be focused
along a line in the θ focal plane with a dispersion
of 1.622 cm/mrad. The position of a particle in
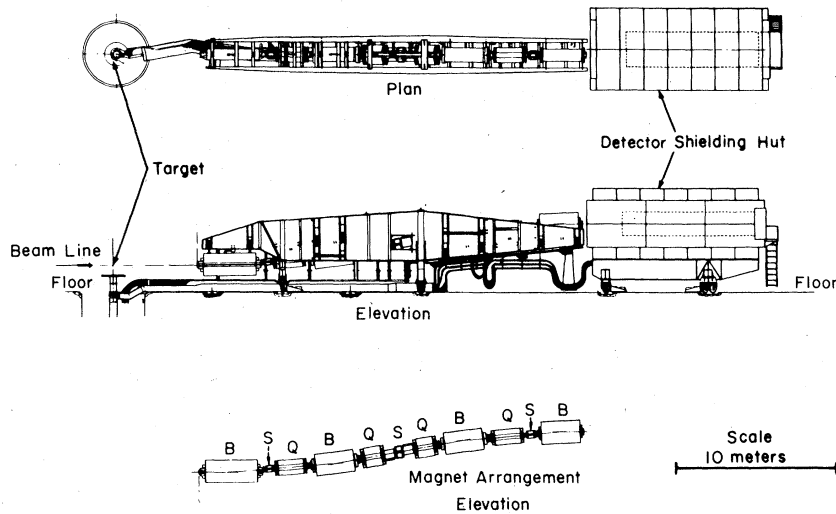this focal plane was measured by the θ hodoscope.

FIG. 3. Plan and elevation view of the SLAC 20-GeV/c spectrometer. The magnet arrangement is shown at the bottom of the figure with the symbols B, Q, and S representing dipole, quadrupole, and sextupole magnets, respectively.

A second point on the horizontal plane trajectory was measured by the X hodoscope, located 4.44 m upstream of the θ hodoscope. In addition to determining the horizontal production angle, information from these two hodoscopes was combined to determine the horizontal angle of the ray through the detection system, the target coordinate perpendicular to the beam in the horizontal plane, and the horizontal coordinate of the ray at the end of the last bending magnet. Cuts were made on these quantities to remove spurious events. Typically, about 5% of the triggers were removed by these cuts.

In the vertical, momentum-dispersing plane the spectrometer is point-to-point focusing. An "S"-shaped double bend with a momentum crossover midway along the spectrometer is used so the central ray leaving the last bending magnet is horizontal. Particles leaving the target with a given momentum are focused along a line in the momentum focal plane with a dispersion of 3.259 cm/%. The δ hodoscope measures the position in this plane.

There is an approximate vertical production angle focus 5.5 m upstream of the momentum focus, where the ϕ hodoscope is located. In addition to determining the particle momentum, information from the ϕ and δ hodoscopes was combined to determine the vertical production angle and the vertical angle of the ray through the detection system. Satisfactory separation between pions and kaons in the differential Cherenkov counter required rejection of events with a vertical angle in the counter greater than 16 mrad. Typically, fewer than 1% of the triggers were eliminated by this requirement.

The photon beam spot at the target is imaged onto the momentum focus with a magnification of 1.35. Thus, to improve the momentum resolution, the vertical size of the beam should be kept small. Some of the data presented here were taken with a reduced beam height to aid in separating the reactions $\gamma p \rightarrow K^+\Lambda$ and $\gamma p \rightarrow K^+\Sigma^0$.

2. Magnet control and momentum scanning

To set the spectrometer to a given central momentum, the proper current in each magnet was calculated, set, and the measured value checked, by an on-line XDS 9300 computer. Current measurement was done with both precision shunts and transductors. The current values were calculated under the assumption that the magnets had a specified recent history, a requirement we did not in general satisfy. This led to a slight disagreement between the momentum calibration of the spectrometer and the electron beam transport system. The fitting programs, discussed below, employed one parameter to accommodate this small difference.

The momentum acceptance of the spectrometer was not large enough to cover, with a single setting of the central momentum, the entire missing-mass region we wished to study. Since adding data taken with different central momenta can be a source of systematic error, due to the imperfect knowledge of the spectrometer acceptance, we adopted the technique of momentum scanning, developed by Boyarski[24] to minimize such errors.

In this method, the spectrometer acceptance was divided into bins of constant missing mass squared, as discussed in Appendix A. Short runs were taken with the spectrometer central momen-
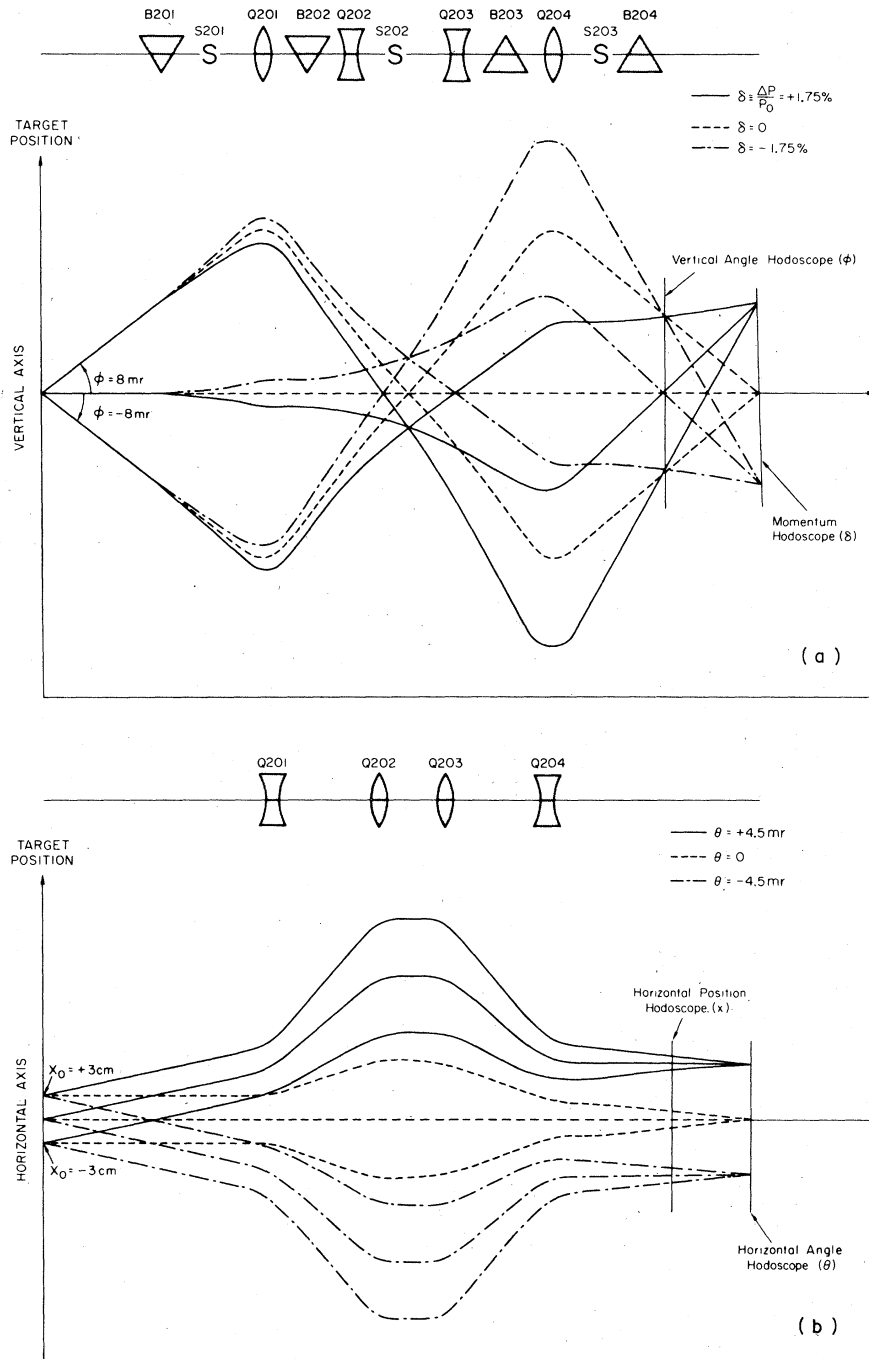
FIG. 4. Calculated trajectories through the spectrometer for selected initial values of horizontal and vertical angles (θ and ϕ), horizontal position (x), and momentum deviation (δ).

tum centered in each missing-mass-squared bin, over the entire missing-mass region to be covered. In this way, the cross section at a given missing mass squared was measured with each part of the spectrometer acceptance.

The procedure followed during a momentum scan was the following:

(1) Data were accumulated for unit of beam flux at a particular spectrometer central momentum. Typically, such a "minirun" lasted 1 minute, and 50 to 60 miniruns were necessary to cover the desired range in missing mass squared.

(2) Upon completion of a minirun the detectors and beam monitors were gated off and commands

were issued to the magnet power supplies to lower the spectrometer central momentum by the width of one missing-mass-squared bin. While the magnets were being set, beam monitors and scalars were read by the computer. Typically, 2 seconds were required to set the new momentum value.

(3) The detectors and beam monitors were gated on, and data were accumulated for another minirun. During the data accumulation, the computer read the shunts and transductors to ensure that the momentum had been correctly set.

3. Event trigger and particle identification

Figure 5 shows a schematic representation of the particle detection system used in this experiment. For most of the experiment, the event trigger was a triple coincidence between the three trigger counters. For data taken at the smallest angle, a shower-counter veto requirement was added to the trigger.

Muons were identified by their penetration of a 14-collision-length iron range telescope, and electrons by their large pulse height in a 17.4-radiation-length lead-Lucite shower counter. Hadrons were defined as those events which did not penetrate the range telescope and which did not produce a large pulse height in the shower counter. The range requirement introduced a negligible inefficiency for hadrons, while the shower-counter pulse-height requirement eliminated 5% of the hadrons.

The threshold Cherenkov counter, which served as the sole identifier of pions among the hadrons, was filled with nitrogen of sufficient pressure for pions to produce Cherenkov light at 28 mrad. The efficiency was 98.2% for negative pions and 98.8% for positive pions. This difference was due to stray magnetic field at the phototube. We estimate that fewer than 3% of the particles identified as pions by the threshold counter were kaons or protons.

The differential Cherenkov counter was used to identify kaons. Light produced in this counter was focused into two annular regions which accepted light between 40 and 60, and 60 and 95 mrad to the central axis, respectively. The inner region was separated into two optically isolated halves, and the outer region into four optically isolated quadrants. Each of these areas was viewed with a separate photomultiplier which was independently pulse-height analyzed. The counter was filled with Freon 13 of sufficient pressure to place the light from pions in the outer ring and that from kaons in the inner region. Protons were below threshold for Cherenkov light production.

Hadrons not identified as pions by the threshold counter were grouped into three classes by the differential counter: kaons, protons, and pions misidentified by the threshold counter. Even though the number of pions in this latter category was small, the larger pion-production cross sections and smaller decay losses could make this a serious background in the kaon yields. By placing conservative cuts on the pulse-height distributions we have eliminated this problem at the expense of kaon identification efficiency. A negligible fraction of our kaon yields were due to misidentified pions, and our overall kaon detection efficiency was 0.937 ± 0.010.

Two small aperture counters were used to study the rate dependence of the trigger. It is particularly important to understand this rate dependence, as it could affect the asymmetry measurements. Since the aperture counters covered only a small fraction of the full acceptance, their counting rate was correspondingly lower than the trigger counters. By measuring the efficiency of the trigger counters for detecting particles which went through the small counters, the normal dead-time monitors (circuits with fixed dead times) were calibrated. The dead-time corrections, made on a minirun by minirun basis were typically less than 2%, and were very nearly identical for data taken with the two beam polarizations.
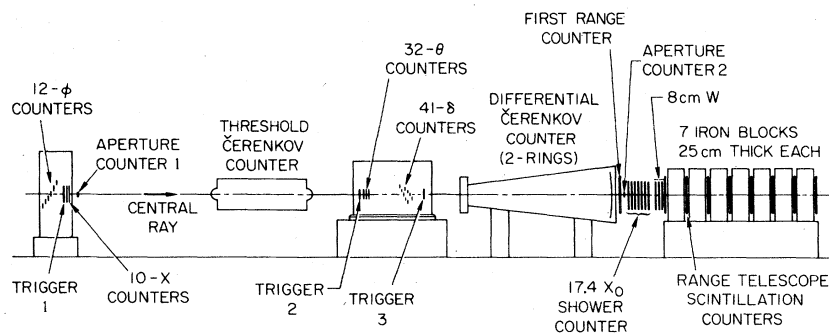

FIG. 5. Detector arrangement in the spectrometer hut.

E. The on-line computer

An XDS 9300 computer, used on line, provided a number of monitor, control, and analysis services. For each event, the computer read and logged on magnetic tape the data from the counters described above. It was possible to read only one event per SLAC beam pulse. A correction for events lost due to this restriction was made by scaling the number of events read by the computer to the number of triggers.

Other tasks performed by the computer included magnet control, polarizer control, monitoring of target temperatures and slit settings, and on-line analysis of the data. Typically, over 80% of all events were analyzed on line, making cross-section and asymmetry results available as data accumulated.

F. Data-taking procedures

Data were taken in sets of four runs, each run consisting of approximately 55 miniruns. The beam polarization was fixed during a run, and each four-run set had two runs of each polarization. The polarization pattern for these four run sets was either ‖-⊥-⊥-‖ or ⊥-‖-‖-⊥ to cancel any linear drifts in the experimental equipment. Between runs, the beam steering was checked, and the polarization changed, if required.

Since the cross sections we measure are momentum dependent, an error in the asymmetry is possible if the central momentum of the momentum bins differed between runs of different polarization. Hysteresis in the spectrometer magnets could be the source of such an error, since in setting the central momentum, the current, rather than the field, was set. Schwitters[25] determined that the magnetic field differed by 0.1% when the spectrometer momentum was cycled up versus cycled down over 10% of the central value. A shift of this magnitude, corresponding to about half a missing-mass-squared bin, could cause a significant error in the measured asymmetries.

For most of the experiment, such hysteresis effects were eliminated by running the spectrometer momentum scans in one direction only. However, the serious nature of this problem was not recognized until some data had been accumulated with the momentum scans done in both directions. The errors on these data have been enlarged to include our estimate of these effects.

Most data were obtained under identical beam, beam monitor, and spectrometer conditions. Deviations from standard beam monitor conditions at 0.3° and 0.7° have already been noted. For the 0.3° running, the trigger was modified by adding a shower-counter veto, and a lead jaw on the

small-angle side of the spectrometer, midway through the magnetic system, was moved into the horizontal aperture to reduce the rate from electron pair production.

III. DATA REDUCTION

A. Cross-section determination

For a given minirun, the counts in any momentum bin may be due to more than one reaction, and the photons which produced these counts can be from any kinematically accessible portion of the spectrum. The experimentally measured result is the cross section per equivalent quantum differential in the solid angle and momentum acceptance of the bin,

$$\text{counts} = \frac{d^2\sigma}{Qd\Omega dp/p} \left(\Delta\Omega \, \frac{\Delta p}{p} \right) N_A N_{EQ} \epsilon \,,$$

where Q indicates the cross section is per equivalent quantum, $\Delta\Omega$ and Δp are the solid angle and momentum acceptance of the bin, N_A the number of target nucleons/cm^2, N_{EQ} the number of equivalent quanta, and ϵ the detection efficiency. This efficiency refers to particle type only, and does not include any bin-to-bin efficiency variations because these are included in the acceptance.

It is convenient to relate the above cross section to one differential only in solid angle by

$$\frac{d\sigma}{d\Omega} = \frac{d^2\sigma}{Qd\Omega dp/p} \left[p \, \frac{dk}{dp} \, n(K) \right]^{-1} , \qquad (2)$$

where dk/dp is the Jacobian relating detected-particle momentum and incident-photon energy and $n(K)$ is the photon flux (see Sec. II A) evaluated at $K = E_0 - 0.05$ GeV.[26] We use this definition of cross section and the convention of evaluating quantities at K when presenting our results. Our measurements of N_A and N_{EQ} were discussed in Sec. II, where many of the necessary corrections to the detection efficiency were also covered. Details on various other corrections necessary in determining the cross sections have been discussed in Ref. 22, and are summarized in Table I for each particle-type and target combination.

The acceptance of each of the 20 missing-mass-squared bins were determined by obtaining the relative acceptances of these bins and the acceptance of the full aperture. A technique adapted from that of Schwitters[25] was used to determine the relative acceptances. The cross section for a given detected particle momentum, p_0, was measured by each of the 20 bins as a consequence of the momentum scanning. The number of counts when this cross section was measured by bin i is directly proportional to the cross section (which is independent of i), the acceptance of the bin

TABLE I. Corrections for detection inefficiencies (not including dead times).

Source of lost events		Correction
Hodoscope inefficiency (blank hodoscopes, undecodable patterns, extra tracks)		1.081 ± 0.020
Failure to reach first range counter due to interaction in the differential counter		1.026 ± 0.006
Hadron identified as an electron by shower counter		1.055 ± 0.006
γ-ray loss in target and material	H_2	1.059 ± 0.005
upstream of target	D_2	1.067 ± 0.005
Absorption of hadrons in target	π, H_2	1.050 ± 0.010
	π, D_2	1.117 ± 0.020
	K, H_2	1.036 ± 0.010
	K, D_2	1.082 ± 0.020
Absorption of hadrons in counters		1.073 ± 0.010
Threshold-Cherenkov-counter inefficiency	π^+	1.012 ± 0.005
or misidentification	π^-	1.018 ± 0.005
	K	1.025 ± 0.005
Differential-Cherenkov-counter inefficiency	K	1.042 ± 0.010
Decay in flight (p is the momentum in GeV)	π	$\exp(46.8/55p)$
	K	$\exp(46.8/7.5p)$
Typical total corrections	π, H_2	1.50 ± 0.03
	π, D_2	1.60 ± 0.03
	K, H_2	2.20 ± 0.03
	K, D_2	2.30 ± 0.03

(which is independent of p_0), and the measured flux factors for the particular minirun. Assuming for convenience of discussion that these flux factors were equal for all miniruns, and denoting them as F_{flux}, one has for the mean number of counts expected

$$\mu(i, p_0) = \frac{d^2\sigma(p_0)}{Qd\Omega dp/p} \left(\Delta\Omega \frac{\Delta p}{p} \right)_i F_{flux} .$$

The unknowns in the problem are the cross sections and bin acceptances. The likelihood for observing these data is

$$\mathcal{L} = \prod_i \prod_{p_0} [\mu(i, p_0)^{c(i, p_0)}] \left\{ \frac{\exp[-\mu(i, p_0)]}{c(i, p_0)!} \right\},$$

where $c(i, p_0)$ is the number of counts observed. By constraining the total acceptance to be a constant, the maximum-likelihood problem can be solved by use of Lagrange multipliers. The relative acceptances determined in this way for all runs at one spectrometer angle were averaged to give the relative bin acceptance for each angle setting.

The acceptance of the full aperture was determined by a combination of experimental and Monte Carlo techniques. This is necessary because of the physical complexity of the spectrometer. There are a number of apertures throughout the spectrometer magnetic system, some of the magnetic elements differ noticeably from ideal behavior, and the spectrometer frame is not perfectly

rigid, allowing the relative positions of the magnets to vary somewhat with spectrometer angle.

Our procedure was to use the hodoscopes to define a small stringent acceptance, unrestricted by any apertures. The acceptance of this stringent region was obtained by calculation, using the measured transport matrix elements of the spectrometer. The full acceptance was then measured relative to the calculated stringent acceptance by lowering the spectrometer momentum to a value where the particle yield did not depend strongly upon momentum or angle, and comparing the number of counts in the full and stringent acceptances.

The acceptance of the stringent region was calculated by tracing randomly generated rays through the spectrometer elements. The ray-tracing program[27] used the best-available model of the spectrometer elements, and included all physical apertures. This calculation verified that the stringent acceptance was not limited by any aperture and was independent of the central angle of the spectrometer to within $\pm 2\%$. The calculation further predicted the ratio of the full-to-stringent acceptances should be of the form $a + b \sin^2\theta_0$, where θ_0 is the central angle of the spectrometer. Our measurements of this ratio are consistent with this behavior.

The value we obtain for the stringent acceptance is 3.6% smaller than that obtained by Boyarski et al.,[28] who followed a similar procedure, and remains an unresolved normalization difference
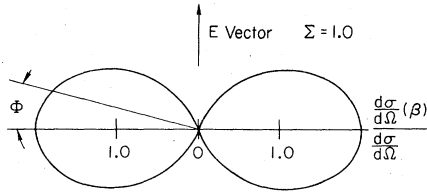
FIG. 6. Polar-angle plot of the cross section versus β, the angle between the electric vector and the production plane, for a process with $\Sigma = 1$. The spectrometer averages over a range in angle Φ.

between these experiments. We estimate the overall uncertainty in our determination of the full acceptance to be $\pm 4\%$.

B. Asymmetry determination

In an experiment such as ours, in which the detector was fixed and the photon polarization vector was rotated, the azimuthal acceptance of the detector must be included in determining the asymmetry. If β is the angle between the photon polarization vector and the production plane, the cross section is given by

$$\frac{d\sigma}{d\Omega}(\beta) = \frac{d\sigma}{d\Omega}\left[1 - \Sigma(t)\cos2\beta\right],$$

where

$$\frac{d\sigma}{d\Omega} = \frac{1}{2}\left[\frac{d\sigma_\perp}{d\Omega} + \frac{d\sigma_\parallel}{d\Omega}\right]$$

is the unpolarized photon cross section, and $\Sigma(t)$ is the asymmetry defined in Eq. (1). The situation is illustrated in Fig. 6.

If Φ is the azimuthal angle between the production plane of a particular event and the central production plane (defined by the incident beam direction and the central ray to the spectrometer aperture), then the cross sections measured with parallel and perpendicular polarized photons are

$$\left\langle\frac{d\sigma}{d\Omega}\right\rangle_\parallel = \frac{d\sigma}{d\Omega}\left[1 - \Sigma(t)\frac{\int A(\Phi)\cos2\Phi\,d\Phi}{\int A(\Phi)d\Phi}\right]$$
$$= \frac{d\sigma}{d\Omega}\left[1 - \Sigma(t)\langle\cos2\Phi\rangle\right]$$

and

$$\left\langle\frac{d\sigma}{d\Omega}\right\rangle_\perp = \frac{d\sigma}{d\Omega}\left[1 + \Sigma(t)\langle\cos2\Phi\rangle\right],$$

where $A(\Phi)$ is the azimuthal acceptance of the spectrometer. The best measurement of $\langle\cos2\Phi\rangle$, defined above, is the weighted mean of the values obtained with parallel and perpendicular photons. Denoting these quantities by $\langle\cos2\Phi\rangle_\parallel$ and $\langle\cos2\Phi\rangle_\perp$,

$\langle\cos2\Phi\rangle$

$$= \frac{\langle d\sigma/d\Omega\rangle_\perp\langle\cos2\Phi\rangle_\perp + \langle d\sigma/d\Omega\rangle_\parallel\langle\cos2\Phi\rangle_\parallel}{\langle d\sigma/d\Omega\rangle_\perp + \langle d\sigma/d\Omega\rangle_\parallel},$$

and, therefore,

$$\Sigma(t) = \frac{\langle d\sigma/d\Omega\rangle_\perp - \langle d\sigma/d\Omega\rangle_\parallel}{\langle d\sigma/d\Omega\rangle_\perp\langle\cos2\Phi\rangle_\perp + \langle d\sigma/d\Omega\rangle_\parallel\langle\cos2\Phi\rangle_\parallel}. \quad (3)$$

Equation (3) gives the asymmetry in terms of the measured cross sections and values for $\langle\cos2\Phi\rangle$. The unpolarized cross section in terms of the measured cross section is

$$\frac{d\sigma}{d\Omega} = \frac{1}{2}\left[\left\langle\frac{d\sigma}{d\Omega}\right\rangle_\perp + \left\langle\frac{d\sigma}{d\Omega}\right\rangle_\parallel\right]. \quad (4)$$

Knowledge of the vertical and horizontal production angles from the hodoscopes was used to determine the azimuthal angle for each event, and from these measurements $\langle\cos2\Phi\rangle$ was determined. Typical values for $\langle\cos2\Phi\rangle$ ranged from 0.67 at a spectrometer angle of $0.7°$ to 0.99 at a spectrometer angle of $4.5°$. The error in $\langle\cos2\Phi\rangle$ was a negligible contribution to the error in the asymmetry.

C. 0.3° analysis

At the $0.3°$ point, the full spectrometer acceptance extended very nearly to $0°$ in the polar angle and included a very large region in azimuthal angle. Since both the cross section and asymmetry for photoproduced pions varies dramatically over this region, it was necessary to subdivide the acceptance to extract meaningful results. To this end, the full acceptance was separated into three polar angle (θ_s) and nine azimuthal angle (Φ_s) regions. The $0.3°$ acceptance, as subdivided, is shown in Fig. 7. Data from the nine azimuthal-angle regions were added symmetrically about the horizontal midplane of the spectrometer to form five $15°$-wide azimuthal bins. The kaon data from the three polar angle bins were averaged, since the kaon yields do not vary strongly over the acceptance at this point.

In principle, the relative acceptances of the 20 missing-mass-squared bins may differ in each (θ_s, ϕ_s) bin. However, the data available for determining these relative acceptances could not be divided this finely and still give reasonable error bars. Therefore, in the analysis of the $0.3°$ data, we have assumed that all relative acceptances were equal. The data were consistent with this assumption. Given equal incident beam fluxes for each minirun, the effect of differing relative acceptances is apparent only near the ends of a momentum scan, where all missing-mass-squared bins do not contribute to the data. The quoted uncertainty on the $0.3°$ results includes a contribu-
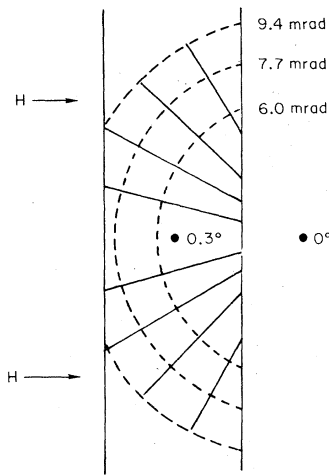
FIG. 7. Spectrometer acceptance for the 0.3° point. Counts with a polar angle greater than 9.4 mrad are not used. The azimuthal angle bins, after folding about the horizontal midplane of the spectrometer, are each 15° wide. The horizontal acceptance is flat within the aperture used and the vertical acceptance is bell shaped with half-maximum points indicated by "H" in the figure.
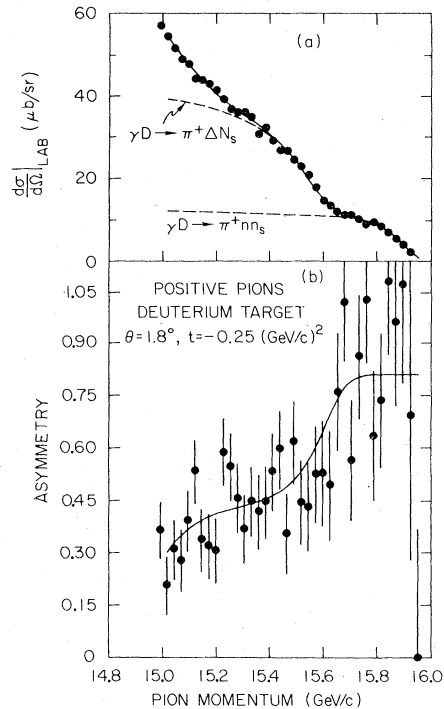

FIG. 8. Typical (a) cross-section and (b) asymmetry momentum distributions for pion photoproduction. The lines are fits described in the text. The contributions of single-pion and $\pi\Delta$ photoproduction to the cross section are shown (n_s and N_s mean spectator neutron and nucleon, respectively).

tion to the error to account for possible differences in the relative acceptances.

For each (θ_s, ϕ_s) bin, an experimental asymmetry was obtained as a function of missing mass squared. These asymmetries were divided by $\langle\cos2\Phi\rangle$ for the particular bin, and a weighted average for the five experimental asymmetries thus obtained at each polar angle was used for the final fitting. An unpolarized cross section was obtained by summing the counts in the five azimuthal-angle bins and averaging over the incident beam polarization. Given the cross section and asymmetry as a function of missing mass squared for each of the three polar-angle bins, fits for the cross section and asymmetry for specific processes were made as for the rest of the data.

These procedures for the small-angle data had the advantages that knowledge of the acceptance of the individual azimuthal-angle bins was not necessary, and that the relative acceptance of the three polar-angle bins does not enter into the final asymmetries. We report values for the pion asymmetry at three angles, and an average kaon asymmetry from our analysis of the 0.3° data.

IV. ANALYSIS OF THE MOMENTUM DISTRIBUTIONS

For each combination of target, spectrometer angle, and spectrometer polarity, the cross section and $\langle\cos2\Phi\rangle$ were measured as a function of momentum. These measurements were made for both photon polarizations and for pions and kaons. The asymmetries and unpolarized cross sections were then obtained from relations (3) and (4).

Typical results for pions are shown in Fig. 8 along with fits to these data.

The dependence of the particle yields on the spectrometer momentum is predominantly a consequence of the beam energy spectrum and two-body kinematics. If the beam were monochromatic and the detected particle was recoiling against a fixed missing mass, the yield would have a sharp spike at a momentum given by two-body kinematics. For a fixed momentum transfer, this momentum depends on the particle masses and the beam energy. On the other hand, a continuous beam spectrum produces a continuous detected particle momentum spectrum. A rapid variation in the beam spectrum has some of the features of the monochromatic beam. For example, the "step" which occurs at the end point of the attenuated bremsstrahlung spectrum [see Fig. 2(b)] produces similar steps in the particle yield for each possible two-body process. The step in the pion yield from the process $\gamma p \to \pi^+ n$ is clearly visible in Fig. 8. The rate of rise of a particular step is determined by (i) the rate of rise of the photon beam at the end point, (ii) the spectrometer resolution, (iii) the natural width of the recoil mass, and (iv)

Fermi motion of the target nucleons in the case of a deterium target.

Processes without a fixed recoiling missing mass also contribute to the yield. These contributions, however, do not reflect the step in the beam spectrum, but rather rise smoothly from their kinematic thresholds as the available phase space increases.

The asymmetry measured at any particular momentum is that of the total yield, and thus contains contributions from all allowed processes. At a given momentum, the contribution of a process to the asymmetry depends on its contribution to the yield. Therefore, to determine the asymmetry of any process, it was necessary to simultaneously fit the average cross section and asymmetry distributions. The free parameters for these fits were the asymmetry and unpolarized cross sections for each process, the experimental resolution and an overall energy shift (see Section II D 2).

A. Fitting the pion data

A χ^2-minimization program[29] was used to determine simultaneously the cross sections and asymmetries for π-N, π-Δ, π-$N(1520)$, and elastic ρ production. The π-$N(1520)$ process was included only where allowed by isospin conservation. Details of the parametrizations used for the photon beam spectrum, the nucleon resonance shapes, the shape of the steps in the case of a sharp recoil mass, and the ρ-production background are given in Appendix B.

Pions of the highest momentum arise from the reaction $\gamma N \to \pi N$. The spectrometer resolution and the sharpness of the step at the end point of the beam spectrum are such that the yield from this process is nearly at its full value before any other process contributes significantly. Thus, results for this reaction are relatively easily extracted. The only difficulty occurs in the case of large momentum transfer and a deuterium target, where the Fermi motion effectively broadens the momentum resolution. The errors shown include the uncertainties introduced by this effect.

Pions from the decay of diffractively photoproduced ρ's and from nonresonant double pion production can contribute to the yield in the region where we extract our π-Δ results. Pions from ρ decay are not a serious background, however, because at the photon energies of this experiment the ρ and Δ bands in the Dalitz plot do not overlap, as shown in Fig. 9. Only ρ's with a mass much greater than the central ρ mass can contribute pions in our region of interest. As noted in Appendix B, we have included a parametrized ρ decay background in our fits to the pion yield.

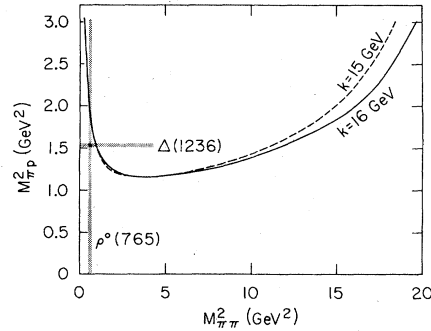The contribution from nonresonant double pion

FIG. 9. Dalitz-plot boundary for $\gamma p \to \pi^+ \pi^- p$. The overlap between the ρ and Δ bands occurs outside the boundary.

production is small, and consequently poorly determined by our measurements. The uncertainties on the cross section and asymmetry for this process, as determined by the fitting procedure, are much larger than one would estimate from the data of other experiments. Including such a background in our fits thus increases the uncertainties on the π-Δ results unreasonably. We have therefore not included any nonresonant double pion production in our fits, but rather have made a liberal estimate of the possible contribution of this process to our pion yields, assigned a 100% error and an asymmetry of 0.0 ± 0.6 to this estimate, and included these effects in our overall error bar. The small size of the estimated effects, discussed below, make this a reasonable procedure.

We have used the SLAC-Berkeley-Tufts (SBT) bubble-chamber results[30] for the total $\gamma p \to \pi^+ \pi^- p$ cross section, subtracted their $\gamma p \to \pi \Delta$ and "parametrization" $\gamma p \to \rho p$ total cross sections, and taken the remainder as the nonresonant double pion total cross section. These results, shown in Fig. 10, are reasonably represented as
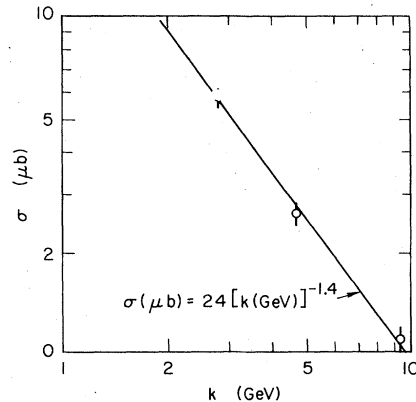

FIG. 10. The nonresonant cross section for $\gamma p \to \pi^+ \pi^- p$. The line is a parametrization used in estimating background contributions from nonresonant pion production. The data are from Ref. 30.
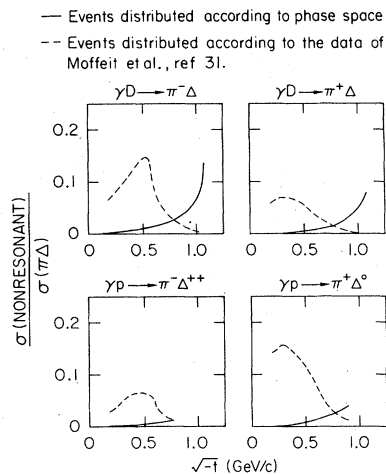
— Events distributed according to phase space

-- Events distributed according to the data of
    Moffeit et al., ref 31.

FIG. 11. The ratio of the cross sections for nonreso-
nant two-pion production to $\pi\Delta$ production in the momen-
tum region used to determine the $\pi\Delta$ cross section and
asymmetry. This ratio is evaluated two ways; by assum-
ing the events are distributed according to phase space
and by assuming they are distributed according to the
results of Moffeit et al. (Ref. 31).

$\sigma_{\text{nonresonant}} = 24k^{-1.4}$ μb with k in GeV, and we use
this expression to estimate the total cross section
at 16 GeV. Similar data for the other double pion
channels are not available; we estimate these
cross sections to be equal to the $\gamma p \to \pi^+\pi^-p$ cross
section.

At 16 GeV, we estimate the nonresonant cross
section for $\gamma p \to \pi^+\pi^-p$ as approximately four times
that for $\gamma p \to \pi^-\Delta^{++}$. However, these cross sections
have very different distributions in the available
phase space. We have used two different distribu-
tions for the nonresonant process to estimate the
contribution to our yields. The first is the as-
sumption that the nonresonant events are distribu-
ted in mass and four-momentum transfer uniformly
in phase space. This assumption leads to larger
backgrounds at large $|t|$. The second was the
measured distributions in x (the Feynman scaling
variable) and transverse momentum.[31] This pro-
cedure leads to larger backgrounds at small $|t|$.
In Fig. 11, the ratio of the nonresonant double
pion contribution to our π-Δ cross section is plot-
ted. In calculating the contribution of this nonre-
sonant production to the error in the π-Δ cross
sections and asymmetries, we have used the larg-
er of the two estimates.

The magnitude we find for the ratio of nonreson-
ant two-pion production to π-Δ production is con-
sistent with what one would expect from the Drell
model.[32] In this model, the cross section for γN
$\to \pi\Delta$ is proportional to the π-N total cross section
at the energy of the exchanged pion. In the region
of the Δ, the π-N total cross section is dominated
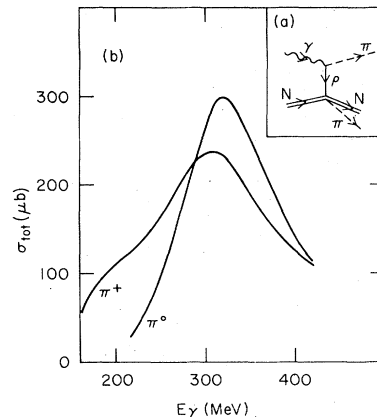

FIG. 12. (a) Model for pion photoproduction via ρ ex-
change. Making the assumptions discussed in the text,
the cross section in this model is proportional to the
total photoproduction cross section at low energy. (b)
The smoothed data from von Holtey (Ref. 33) shows a
low-mass enhancement in the π^+ total cross section.

by the Δ, and the nonresonant cross section is
much smaller than the Δ cross section.

An alternative way to view photoproduction for
the purpose of considering backgrounds is related
to the ρ-exchange diagram of Fig. 12(a). Neglect-
ing off-mass-shell effects and the contribution of
longitudinal ρ's, equating charged-ρ and neutral-ρ
exchange, and using vector dominance, one has a
cross section for ρ exchange which is proportional
to the total photoproduction cross section (at an
energy equal to the energy of the exchanged ρ).
The tenuous nature of the theoretical argument
negates the value of a detailed calculation, but the
argument does suggest that the missing-mass dis-
tribution in high-energy photoproduction may be
related to the total photoproduction cross section
at low energies.

These cross sections are presented in Fig.
12(b)[33]; one sees that the π^+ cross section has a
structure other than the Δ at low energy. Both the
energy dependence and the angular distribution in-
dicate that this structure is a nonresonant S-wave
contribution to the cross section.[34] Such a struc-
ture in our measured missing-mass distributions
would affect some of our results.

We have studied the shape and other features of
our measured momentum distributions, but our
resolution in missing mass is inadequate to give a
conclusive answer concerning the existence of any
such background. The tests we performed indicate
that enhancements at low missing mass are not
present, however, and thus in our analysis we
have assumed the effect is absent. The measure-
ments of cross sections and small magnitude as-
ymmetries for $\gamma p \to \pi^+\Delta^0$ and $\gamma n \to \pi^-\Delta^+$ are most
sensitive to this assumption.

B. Fitting the kaon data

Just as the pion data can be characterized by π-N, π-Δ, and multipion production, the kaon data are described by K-Λ, K-Σ, and a background without a fixed recoiling missing mass. This background rises smoothly from the K-π^0-Λ threshold. A K^+ yield curve, together with the π^+ yield measured at the same time, is shown in Fig. 13. The cross section above the K-Λ threshold is negligible indicating that pions are not a serious background to the kaon data.

The K-Λ and K-Σ reactions are not observed as separate steps; the resolution smears these steps together. Comparison of the rates of rise to the π^+ step and the K^+ step clearly indicates the presence of more than one contribution to the K^+ step. Since the pion and kaon yields were measured at the same time, the contributions of beam steering, beam size, and magnet hysteresis to the momentum resolution and offset were the same for both sets of data. Without the information about the resolution and offset from the pion data, it would be impossible to separate the K-Λ and K-Σ reactions. In fitting the kaon data, the pion data were used to determine these two quantities. Even with this additional information, the separation of K-Λ from K-Σ cross sections is tenuous, and the resultant separation has large correlated errors, since the sum of the two cross sections is well determined. The errors in the individual asymmetries are further magnified by the small beam polarization. We have carefully checked our pro-

cedures for handling the correlated errors, and have included the effects of uncertainties in the momentum resolution and offset in our results for the separated reactions.

The sum of the K-Λ plus K-Σ cross sections is not affected by the percentage of the step attributed to the individual reactions. The most significant uncertainty in the determination of the cross section and asymmetry of this sum is the character of the lower momentum background. Fortunately, no backgrounds are kinematically possible over most of the region where the step rises; the sum of the two cross sections is rather well determined and is not sensitive to the background parametrization chosen.

V. RESULTS AND DISCUSSION

A. Single-pion photoproduction

Our results for single-pion photoproduction from hydrogen and deuterium targets are presented in Tables II, III, and IV. Some of these results have been published previously.[5]

The ratio of our measured cross sections for $\gamma p \rightarrow \pi^+ n$ to those of Boyarski *et al*.[35] is 1.19 ± 0.03. This ratio shows no t dependence within the quoted error. Known t-independent differences in the analysis of the two experiments account for 0.08 of this ratio, leaving an unaccounted normalization difference of 1.11 ± 0.03. We estimate our overall normalization uncertainty to be 0.07, while that of Boyarski *et al*.[35] was given as 0.06. In Fig. 14, we compare our measurements for the ratio R between the cross sections for $\gamma D \rightarrow \pi^- p p_s$ and $\gamma D \rightarrow \pi^+ n n_s$ with those of Boyarski *et al*.[36] (p_s and n_s denote a spectator proton and neutron, respectively.) The agreement between the two experiments is excel-
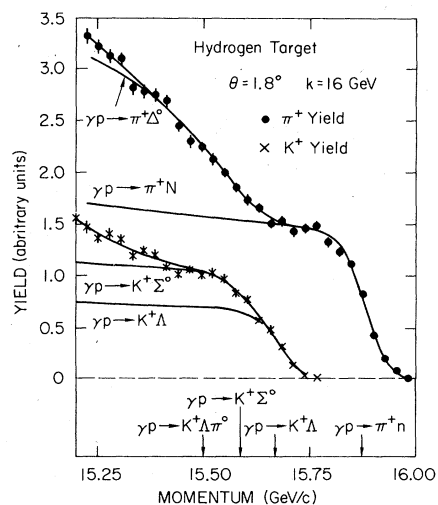

FIG. 13. Yields for pion and kaon photoproduction. The step for single-pion photoproduction is clearly steeper than the combined $K^+\Lambda$, $K^+\Sigma^0$ step. Any momentum shift and the momentum resolution were determined from the pion data. Thresholds for various reactions are indicated by the arrows.

TABLE II. Cross-section and asymmetry results for $\gamma p \rightarrow \pi^+ n$ at 16 GeV.

$-t$ [(GeV/c)^2]	$d\sigma/dt$ [μb/(GeV/c)^2]	Σ
0.0055	a	0.27 ± 0.09
0.0122	a	0.55 ± 0.08
0.0173	a	0.78 ± 0.19
0.0337	0.185 ± 0.006	1.01 ± 0.05
0.0530	0.152 ± 0.010	1.02 ± 0.05
0.0826	0.147 ± 0.007	0.89 ± 0.09
0.155	0.136 ± 0.006	0.80 ± 0.04
0.257	0.113 ± 0.003	0.77 ± 0.06
0.418	0.086 ± 0.003	0.74 ± 0.04
0.602	0.0559 ± 0.0023	0.88 ± 0.05
0.826	0.0297 ± 0.0010	0.93 ± 0.04
1.499	0.0028 ± 0.0003	1.13 ± 0.13

[a] The analysis of these data points did not give absolute cross sections.

TABLE III. Results for $\gamma D \to \pi^+ nn_s$.

$-t$ [(GeV/c)^2]	$\dfrac{d\sigma/dt \ (\gamma D \to \pi^+ nn_s)}{d\sigma/dt \ (\gamma p \to \pi^+ n)}$	Σ
0.0055	a	0.19 ± 0.12
0.0122	a	0.47 ± 0.13
0.0173	a	0.69 ± 0.17
0.0337	0.93 ± 0.06	1.02 ± 0.13
0.0530	0.86 ± 0.06	0.96 ± 0.12
0.0826	0.99 ± 0.04	1.07 ± 0.12
0.155	1.00 ± 0.06	0.67 ± 0.11
0.257	1.09 ± 0.05	0.82 ± 0.07
0.418	1.08 ± 0.07	0.86 ± 0.06
0.602	1.00 ± 0.09	0.96 ± 0.07
0.826	1.07 ± 0.08	1.11 ± 0.06
1.193	b	1.08 ± 0.10

[a] The analysis of these data points did not give cross-section ratios.

[b] The cross section for $\gamma p \to \pi^+ n$ was not measured at this t value.

lent over the entire t range. We conclude that any differences between our results and earlier experiments are t independent. We furthermore believe that the small normalization differences between these measurements do not affect our asymmetry measurements in any significant way.

Figure 15(a) shows the ratio of our single-π^+ photoproduction cross sections from hydrogen and deuterium. Since single positive pions can be photoproduced only from the proton of the deuterium nucleus, the value of this ratio tests the adequacy of approximating the deuterium cross sections as the sum of free-proton and free-neutron cross sections. As expected, this ratio falls be-
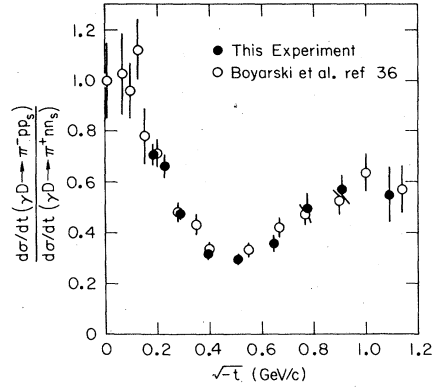

FIG. 14. Comparison of our measurements of the π^-/π^+ ratio made with unpolarized photons and those of Boyarski et al. (Ref. 36).

low unity at small momentum transfers, due to the exclusion principle, and is consistent with one at higher momentum transfers. This comparison indicates that there are no significant systematic errors in isolating single-pion production from deuterium, and that any Glauber scattering or Fermi motion effects are small.

Figure 15(b) compares our measurements of the asymmetries in $\gamma p \to \pi^+ n$ and $\gamma D \to \pi^+ nn_s$. The good agreement obtained indicates we can interpret the asymmetry in $\gamma D \to \pi^- pp_s$ as that from the reaction $\gamma n \to \pi^- p$. Calculations by Julius[37] show that any difficulties with such an interpretation should be small compared with the accuracy of our measurements. These calculations are only weakly dependent upon the photoproduction amplitudes used.
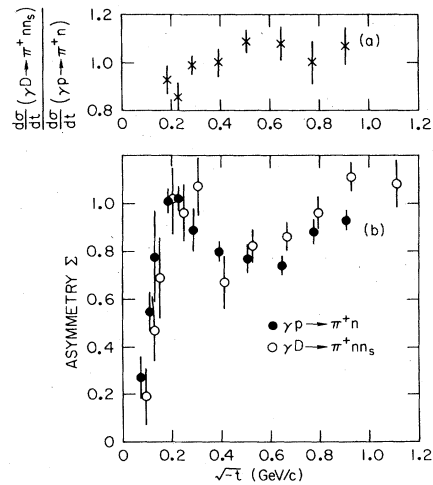
TABLE IV. Results for $\gamma D \to \pi^- pp_s$.

$-t$ [(GeV/c)^2]	$R \equiv \dfrac{d\sigma/dt \ (\gamma D \to \pi^- pp_s)}{d\sigma/dt \ (\gamma D \to \pi^+ nn_s)}$	Σ
0.0055	a	0.04 ± 0.10
0.0122	a	0.38 ± 0.10
0.0173	a	0.59 ± 0.16
0.0337	0.708 ± 0.043	0.98 ± 0.07
0.0530	0.662 ± 0.046	0.91 ± 0.07
0.0826	0.473 ± 0.020	0.57 ± 0.10
0.155	0.318 ± 0.022	0.47 ± 0.07
0.205	b	0.35 ± 0.10
0.257	0.294 ± 0.019	0.55 ± 0.09
0.418	0.357 ± 0.034	0.74 ± 0.07
0.602	0.496 ± 0.058	0.85 ± 0.07
0.826	0.569 ± 0.057	0.94 ± 0.07
1.193	0.55 ± 0.11	1.06 ± 0.11

[a] The analysis for these data points did not give cross-section ratios.

[b] The cross section for $\gamma D \to \pi^+ nn_s$ was not measured at this t value.

FIG. 15. (a) Cross-section ratio for single-π^+ photoproduction from hydrogen and deuterium. (b) Comparison of the single-π^+ photoproduction asymmetry from hydrogen and deuterium.
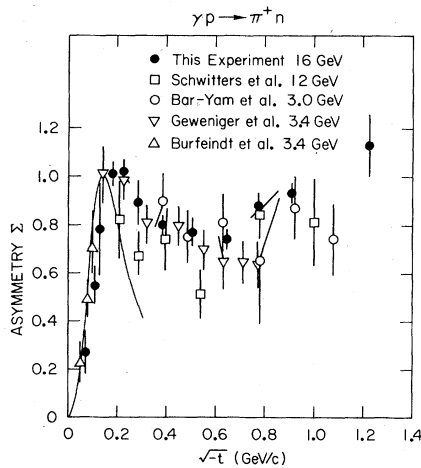
FIG. 16. The polarized-photon asymmetry for single-π^+ photoproduction. In addition to our measurements we show the results of Refs. 7-10. The curve is the asymmetry in the electric Born model.

Julius has used the amplitudes of Kellet[38] which do not describe our results particularly well.

The asymmetry for $\gamma p \to \pi^+ n$, presented with other data in Fig. 16, is seen to have little or no energy dependence over the range of incident photon energies from 3 to 16 GeV. However, the asymmetry in $\gamma D \to \pi^- p p_s$, shown in Fig. 17, shows significant energy dependence.

By parametrizing the differential cross sections for perpendicular and parallel polarized photons
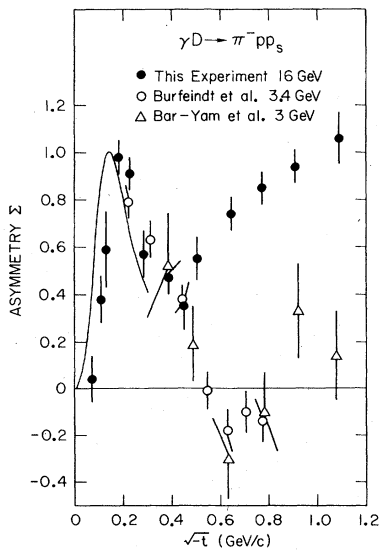

FIG. 17. The polarized-photon asymmetry for single-π^- photoproduction. Also shown are the lower-energy results of Refs. 11 and 12 and the asymmetry in the electric Born model.

in a Regge form:

$$\frac{d\sigma_{\perp,\parallel}}{dt} = f(t) S^{2\alpha_{\perp,\parallel}(t)-2} ,$$

we can calculate the effective Regge trajectories for natural- and unnatural-parity exchanges, respectively. These are given by

$$\alpha^+_{\perp,\parallel}(t) = \alpha^+_0(t) + \frac{\ln\left[\dfrac{1 \pm \Sigma^+(s_2,t)}{1 \pm \Sigma^+(s_1,t)}\right]}{2\ln\left(\dfrac{s_2}{s_1}\right)} ,$$

$$\alpha^-_{\perp,\parallel}(t) = \alpha^+_0(t) + \frac{\ln\left[\dfrac{R(s_2,t)}{R(s_1,t)}\right] + \ln\left[\dfrac{1 \pm \Sigma^-(s_2,t)}{1 \pm \Sigma^-(s_1,t)}\right]}{2\ln\left(\dfrac{s_2}{s_1}\right)} , \quad (5)$$

and

$$\alpha^I_{\perp,\parallel}(t) = \alpha^+_0(t) + \frac{\ln\left[\dfrac{1 \pm \Sigma^+(s_2,t) + R(s_2,t)[1 \pm \Sigma^-(s_2,t)]}{1 \pm \Sigma^+(s_1,t) + R(s_1,t)[1 \pm \Sigma^-(s_1,t)]}\right]}{2\ln\left(\dfrac{s_2}{s_1}\right)} ,$$

where the superscripts $+$, $-$, and I refer to the reactions $\gamma p \to \pi^+ n$, $\gamma n \to \pi^- p$, and their sum, which is the isovector photon cross section; the subscripts $\perp$, $\parallel$, and 0 refer to perpendicular, parallel, and unpolarized photons, the $+$ $(-)$ sign in the $1 \pm \Sigma$ terms is used with perpendicular (parallel) photons, R is the ratio of the differential cross sections for π^- to π^+ photoproduction from deuterium, and s_1 and s_2 refer to the two different c.m. energies used. For these calculations, we have used our data at 16 GeV, the R measurements of Bar-Yam *et al.*[39] at 3 GeV and Heide *et al.*[40] at 3.4 GeV, and the asymmetry measurements of Bar Yam *et al.*[11] at 3 GeV. The low-energy data were linearly interpolated in t where necessary.

Uncertainties in the beam polarization were included in these calculations. Ordinary error propagation was used in the calculations for perpendicular photons. For the case of parallel photons, where $1 - \Sigma$ may be within an error bar of zero, a Monte Carlo technique was necessary. A value for each of the measured quantities on the right-hand side of relations (5) was randomly generated. The distribution of each of the generated quantities was Gaussian, with a mean and standard deviation given by the measurements. The effective trajectory was calculated for each resulting set of values for the quantities. The procedure was repeated 20 000 times. The median of the resulting values for the effective trajectory is given in Fig. 18. The error bars indicate the range containing 68.3% of the values.

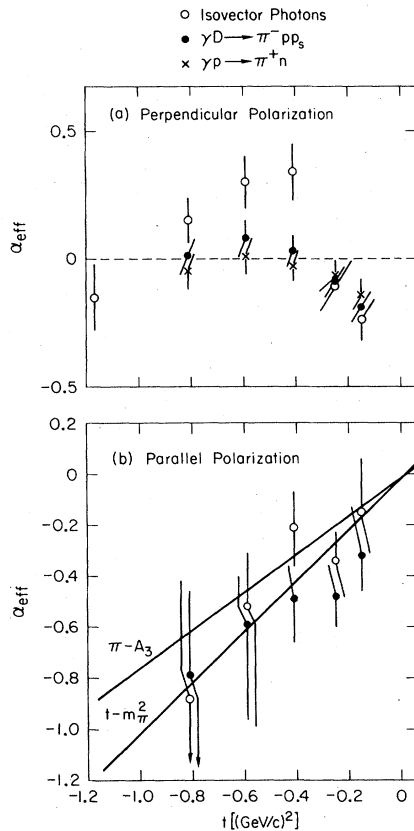The effective trajectory of photoproduction of

FIG. 18. The effective Regge trajectories for (a) perpendicular and (b) parallel polarizations. α_{eff} for perpendicular polarization is roughly consistent with zero, while for parallel polarization it is consistent with either of the two possible Regge trajectories shown.

FIG. 19. The π^-/π^+ ratio for single-pion photoproduction with polarized and unpolarized photons. Also included in the figure are the lower-energy results of Refs. 11 and 12.

single pions with perpendicular photons is close to zero, as is the case with unpolarized photons. With parallel photons, the effective trajectory is consistent with that expected of a conventional pion Regge trajectory of either unit slope, or a slope determined by the pion and A_3 (Ref. 41) masses. Both π and B exchange can contribute to π^- photoproduction with parallel photons. The effect of any energy dependence of π-B interference can be eliminated by calculating the effective trajectory for the sum of π^+ and π^- production. The result, labeled isovector photons in Fig. 18, is similar, consistent with weak π-B exchange degeneracy.

In general, Regge cuts introduced to explain the nonzero forward cross section for single-pion photoproduction would be expected to dominate the energy dependence of the cross section for parallel photons, giving results similar to those with perpendicular photons. This does not appear to be the case. Photoproduction models involving pion conspiracy can explain both the nonzero forward cross section, and the energy dependence of the
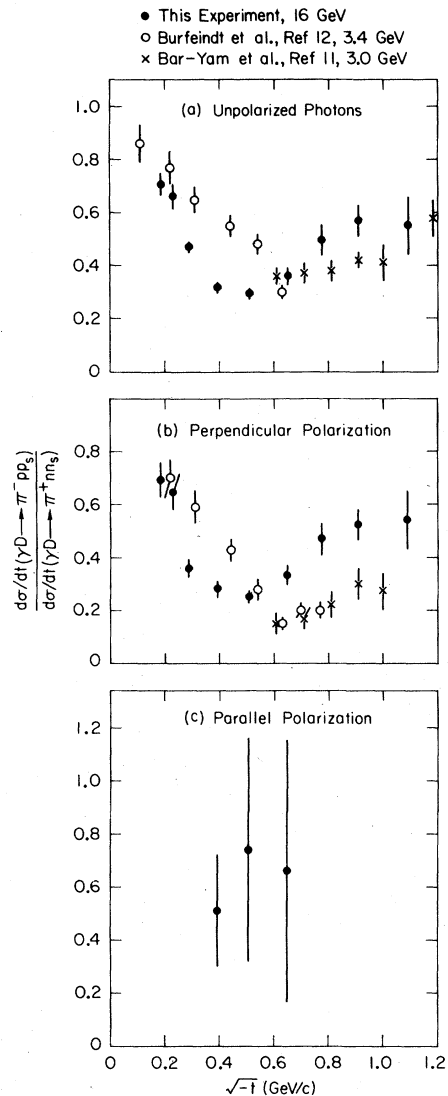
parallel photon cross section.

Lower-energy data have shown that the decrease in R for $|t| \geq 0.1$ $(\text{GeV}/c)^2$ is associated with perpendicularly polarized photons.[39,40] Interference between t-channel exchanges of natural parity and opposite G parity produce this effect. Our data, shown in Fig. 19, indicate that this is the case at 16 GeV also. We see no statistically significant evidence for interference between unnatural-parity exchanges of opposite G parity.

The ratio $R_\perp$ for perpendicular photons has significant energy dependence over the entire t range for which it has been measured. At small $|t|$, this dependence is clear even in the unpolarized photon

TABLE V. Cross-section and asymmetry results for $\pi\Delta$ photoproduction from hydrogen.

| $-t$ [(GeV/c)^2] | $\gamma p \to \pi^+\Delta^0$ | | $\gamma p \to \pi^-\Delta^{++}$ | |
	$d\sigma/dt$ [μb/(GeV/c)^2]	Σ	$d\sigma/dt$ [μb/(GeV/c)^2]	Σ
0.0058	a	-0.28 ± 0.21	a	-0.16 ± 0.08
0.0122	a	-0.33 ± 0.20	a	-0.25 ± 0.08
0.0173	a	-0.52 ± 0.25	a	-0.43 ± 0.19
0.0337	0.426 $\pm$ 0.053	-0.30 ± 0.19	1.039 $\pm$ 0.035	-0.47 ± 0.05
0.0520	0.315 $\pm$ 0.045	-0.59 ± 0.21	0.690 $\pm$ 0.041	-0.64 ± 0.08
0.0816	0.260 $\pm$ 0.040	-0.10 ± 0.21	0.492 $\pm$ 0.024	-0.67 ± 0.10
0.152	0.177 $\pm$ 0.024	0.03 ± 0.20	0.218 $\pm$ 0.013	-0.89 ± 0.14
0.252	0.124 $\pm$ 0.013	0.39 ± 0.16	0.1116 $\pm$ 0.0064	-0.62 ± 0.10
0.408	0.0774 $\pm$ 0.0058	0.89 ± 0.17	0.0732 $\pm$ 0.0026	0.23 ± 0.06
0.592	0.0521 $\pm$ 0.0031	0.85 ± 0.18	0.0531 $\pm$ 0.0013	0.75 ± 0.07
0.806	0.0216 $\pm$ 0.0022	0.88 ± 0.21		

[a]The analysis of these data points did not give absolute cross sections.

data (Fig. 19), while at large $|t|$ the energy dependence of $R_\perp$ is a reflection of that of the π^- asymmetry.

As the reactions $\gamma p \to \pi^+ n$ and $\gamma n \to \pi^- p$ are related by line reversal, their cross sections are expected to become equal asymptotically.[42] Deviation of R from unity is thus an indication that the photoproduction amplitudes have not reached asymptotic behavior. At large $|t|$, R is at least moving toward unity with increasing energy, while at small $|t|$, this ratio is decreasing with increasing energy. It is clear that the natural-parity photoproduction amplitudes in the forward direction are very far from asymptotic behavior at the energy of the present measurements. There is no statistically significant evidence that $R_\parallel$ is different than one at both 3.4 and 16 GeV, and thus one cannot conclude that the photoproduction amplitudes with parallel photons are not asymptotic.

B. π-$\Delta(1236)$ photoproduction

Our cross-section and asymmetry results for the reactions $\gamma p \to \pi^-\Delta^{++}$, $\gamma p \to \pi^+\Delta^0$, $\gamma D \to \pi^-\Delta N_s$, and $\gamma D \to \pi^+\Delta N_s$, where N_s indicates a spectator

nucleon, are given in Tables V and VI. The deuterium reactions represent the sums of the reactions $\gamma D \to \pi^-\Delta^{++}n_s$ plus $\gamma D \to \pi^-\Delta^+ p_s$, and $\gamma D \to \pi^+\Delta^0 n_s$ plus $\gamma D \to \pi^+\Delta^- p_s$, respectively.

The ratio between our measured cross sections and those of Boyarski *et al.*[43] is 1.28 ± 0.07, independent of both reaction and momentum transfer within the stated error. Based on the ratio of measured cross sections for $\gamma p \to \pi^+ n$ and different procedures for normalizing the Breit-Wigner for the Δ (see Appendix B), we expect a ratio of 1.34 ± 0.04 As before, we do not believe that small normalization uncertainties influence our asymmetry results in a meaningful way.

The asymmetry results, plotted in Fig. 20, show that all four reactions are dominated by unnatural-parity exchange at small $|t|$ and natural-parity exchange at large $|t|$. In Fig. 21 we have combined our cross-section and asymmetry measurements to obtain the cross sections for perpendicular and parallel photons.

The unnatural-parity exchange cross sections of all four reactions vary approximately as $e^{11.5t}$ for $m_\pi^2 \le -t \le 0.2$ GeV^2. Since unnatural-

TABLE VI. Cross-section and asymmetry results for $\pi\Delta$ photoproduction from deuterium.

| $-t$ [(GeV/c)^2] | $\gamma D \to \pi^+\Delta N_s$ | | $\gamma D \to \pi^-\Delta N_s$ | |
	$d\sigma/dt$ [μb/(GeV/c)^2]	Σ	$d\sigma/dt$ [μb/(GeV/c)^2]	Σ
0.0337	1.52 $\pm$ 0.11	-0.23 ± 0.11	1.36 $\pm$ 0.10	-0.49 ± 0.09
0.0520	1.008 $\pm$ 0.098	-0.27 ± 0.10	0.851 $\pm$ 0.086	-0.66 ± 0.10
0.0816	0.878 $\pm$ 0.062	-0.20 ± 0.11	0.614 $\pm$ 0.060	-0.68 ± 0.13
0.152	0.547 $\pm$ 0.040	0.19 ± 0.09	0.316 $\pm$ 0.038	-0.75 ± 0.16
0.252	0.361 $\pm$ 0.021	0.28 ± 0.08	0.141 $\pm$ 0.019	-0.41 ± 0.13
0.408	0.244 $\pm$ 0.014	0.57 ± 0.09	0.105 $\pm$ 0.010	0.21 ± 0.11
0.592	0.150 $\pm$ 0.012	0.59 ± 0.11	0.0728 $\pm$ 0.0062	0.55 ± 0.10
0.806	0.0836 $\pm$ 0.0048	0.79 ± 0.09	0.0452 $\pm$ 0.0030	0.78 ± 0.10
1.173	0.0224 $\pm$ 0.0033	0.47 ± 0.18	0.0128 $\pm$ 0.0021	0.76 ± 0.22
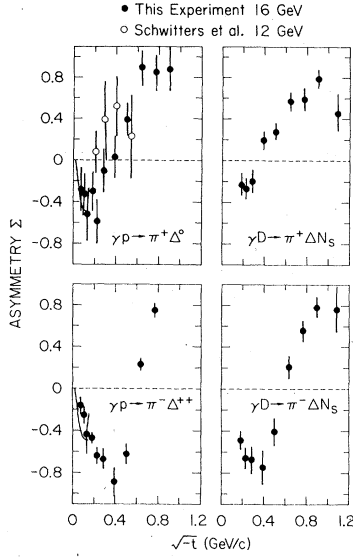
FIG. 20. The polarized-photon asymmetries for $\pi\Delta$ photoproduction. The $\pi^+\Delta^0$ data are compared with the lower-energy data of Ref. 10 and with the minimal gauge-invariant calculation of Ref. 49. This calculation is also compared with the $\pi^-\Delta^{++}$ data.
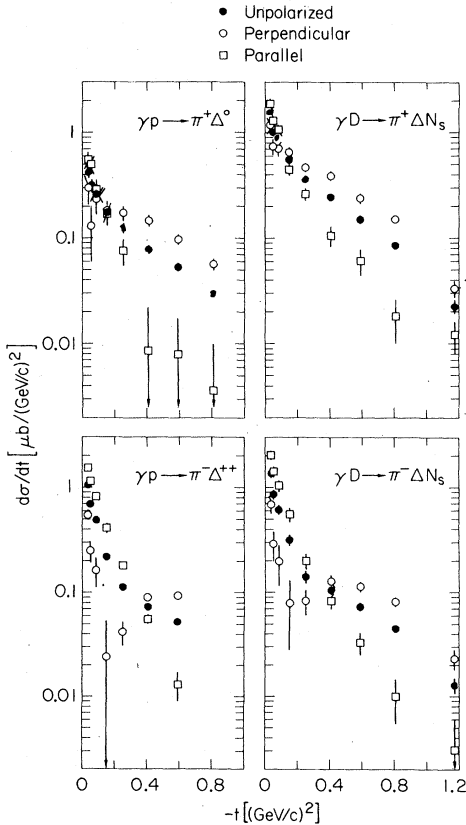

FIG. 21. Cross sections for $\pi\Delta$ photoproduction with polarized and unpolarized photons.

parity exchange is dominant in this t region, the unpolarized photon cross section displays similar t dependence. At large $|t|$ the unnatural-parity exchange cross sections fall as e^{6t} to e^{8t} depending on the particular reaction.

The natural-parity exchange cross sections have considerable reaction-dependent structure in the small-$|t|$ region. Both $\gamma p \to \pi^- \Delta^{++}$ and $\gamma D \to \pi^- \Delta N_s$ have large dips in the cross section for perpendicular photons at $t \simeq -0.15$ GeV/c^2. The presence of a dip at this t value is suggestive of a cross section dominated by net s-channel helicity flip $= 0$. However, when the polarized-photon asymmetry is different from zero, as is the case, there must be more than one s-channel amplitude present. This can be seen by writing the polarized photon asymmetry in terms of the s-channel amplitudes

$$\Sigma = \frac{2\,\mathrm{Re}(H_1 H_6^* + H_2 H_7^* + H_3 H_4^* + H_5 H_8^*)}{\displaystyle\sum_{i=1}^{8} |H_i|^2} \;,$$

where H_1 and H_2 are the helicity-flip-zero amplitudes, H_3, H_4, and H_5 are the helicity-flip-one amplitudes, H_6 and H_7 are the helicity-flip-two amplitudes, and H_8 is the helicity-flip-three amplitude. The asymmetry arises from an interference between different s-channel amplitudes.

Therefore, the cross section for perpendicularly polarized photons

$$\frac{d\sigma_\perp}{dt} \propto \sum_{i=1}^{\infty} |H_i|^2 + 2\,\mathrm{Re}(H_1 H_6^* + H_2 H_7^* + H_3 H_4^* + H_5 H_8^*) \;,$$

can be dominated by a single s-channel amplitude only through a fortuitous cancellation of many terms. A similar dip at about the same t value has been seen in the closely related reaction $\pi^+ p \to \Delta^{++}\rho^0$.[44] This paper shows that a rapid decrease in the absorption-corrected one-pion exchange combined with an increase in the A_2-exchange contribution can explain this observation.

The cross sections for $\pi\Delta$ production in terms of amplitudes with fixed t-channel quantum numbers are[43]

$$\frac{d\sigma}{dt}\begin{pmatrix}\gamma p \to \pi^- \Delta^{++}\\ \gamma n \to \pi^+ \Delta^-\end{pmatrix} = 3\sum_{i=1}^{8} |A_{1-}^i \mp A_{1+}^i - \tfrac{1}{3}A_{2-}^i|^2$$

and

$$\frac{d\sigma}{dt}\begin{pmatrix}\gamma n \to \pi^- \Delta^+\\ \gamma p \to \pi^+ \Delta^0\end{pmatrix} = \sum_i |A_{1-}^i \mp A_{1+}^i + A_{2-}^i|^2 \;, \qquad (6)$$

where the summation is over the eight helicity amplitudes, the subscripts 1 and 2 refer to the
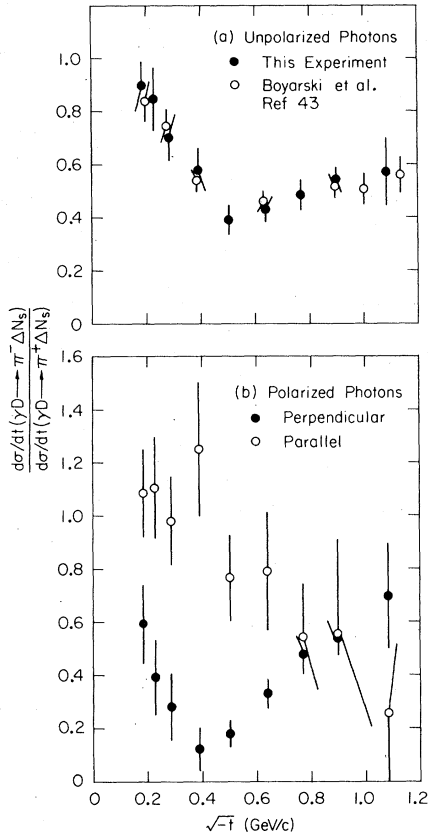
FIG. 22. The π^-/π^+ cross-section ratio for $\Delta\pi$ photoproduction with polarized and unpolarized photons.
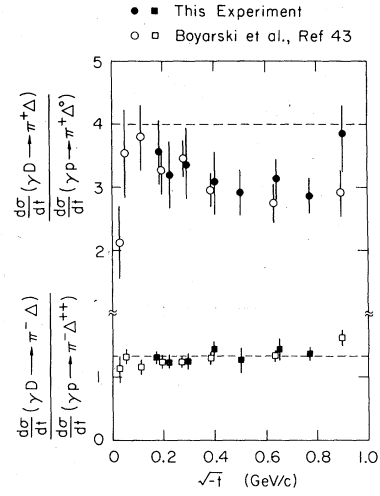

FIG. 23. The deuterium-to-hydrogen cross-section ratios for unpolarized photons compared with those of Boyarski *et al.* (Ref. 43). The dashed lines show the values expected in the absence of $I = 2$ exchanges.

t -channel isotopic spin, and the $+$ and $-$ subscripts denote the G parity of the t channel. Positive G-parity exchanges correspond to isoscalar photons and negative G parity to isovector photons. In the approximation that any $I = 2$ amplitudes are small, the ratio of $\pi^-\Delta$ to $\pi^+\Delta$ production from deuterium depends on the interference of $I = 1$ exchanges of different G parity:

$$R = \frac{(d\sigma/dt)(\gamma D \to \pi^- \Delta N_s)}{(d\sigma/dt)(\gamma D \to \pi^+ \Delta N_s)} \simeq \frac{\sum\limits_{i=1}^{8} |A^i_{1-} - A^i_{1+}|^2}{\sum\limits_{i=1}^{8} |A^i_{1-} + A^i_{1+}|^2} .$$

In Fig. 22(a) we compare our measurement of R for unpolarized photons with that of Boyarski *et al.*[43] The agreement is excellent. In Fig. 22(b) we present our measurements for polarized photons. For parallel photons R is slightly greater than one for $\sqrt{-t} < 0.4$ GeV^2 and falls below one at larger $|t|$. This is an indication of interference between unnatural-parity exchanges of opposite G parity.

The ratio R for perpendicular photons shows that there is significant interference between

natural-parity exchanges of opposite G parity over the entire t region of this experiment. This interference is comparable to that seen in single-pion photoproduction (see Fig. 19) except around $t = -0.15$ GeV.^{2}

Mesons with two units of isospin are exotic, and no such particle has been discovered. However, there is evidence of $I = 2$ t -channel exchanges. Boyarski *et al.*[43] measured the ratios of cross sections for $\pi^-\Delta$ and $\pi^+\Delta$ from deuterium and hydrogen. These ratios should be $\frac{4}{3}$ and 4, respectively, in the absence of $I = 2$ exchanges [see Eqs. (6)]. Our results are compared with theirs in Fig. 23; we agree with their measurements. The π^- data are consistent with the predicted ratio , and the π^+ data are clearly inconsistent.

In Fig. 24 we present these cross-section ratios for perpendicular and parallel photons. Both ratios for $\pi^+\Delta$ production disagree with the expected value of 4. The average ratios are 2.94 ± 0.21 and 2.97 ± 0.34 for perpendicular and parallel photons, respectively. The $I = 2$ exchange does not have a definite parity; this makes Regge cuts the probable explanation.

As discussed in Sec. IV A, we assume that the Δ is the only contribution to the momentum distribution which is rapidly varying near the Δ threshold. If the ρ-exchange model discussed in that section were correct, this would not be the case. In particular, the cross section for $\gamma p \to \pi^+\Delta^0$ would be most strongly affected thereby raising the π^+ deuterium-to-hydrogen ratio closer to the value expected in the absence of $I = 2$ exchanges. Data with better missing-mass resolution are required to rule out backgrounds of this type, and
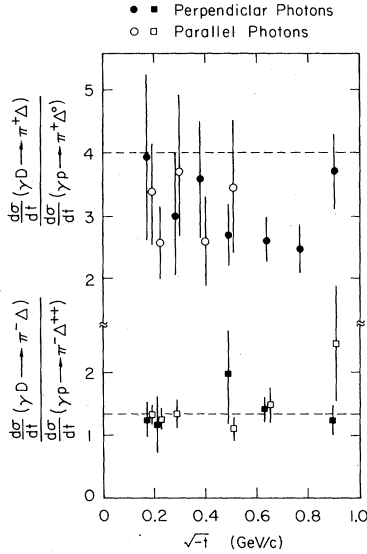
FIG. 24. The deuterium-to-hydrogen cross-section ratios for polarized photons.

therefore, one must be cautious about conclusions related to $I = 2$ exchanges.

Several theoretical models have been developed for π-Δ photoproduction using these polarization data. Goldstein and Owens[45] use Regge poles, absorption corrections, and Regge-Regge cuts. Clark[46] uses a phenomenological extension of amplitudes which are constrained by gauge invariance at low $|t|$.

C. Photoproduction at small $|t|$

The extreme small-angle region in single-pion photoproduction has played a crucial role in the development of theories for this process at high energies. The first measurements[35, 40] discovered that the cross section rises by a factor of 2 in the region between $t \approx -m_\pi^2$ and $t = t_{\min}$, in contrast to the expected dip. The experimenters[35] noted that the cross section in this region agreed approximately in magnitude as well as in t and s dependence with the results of the gauge-invariant electric Born approximation.

In 1964, Stichel and Scholz[47] calculated the minimal gauge-invariant contribution of one-pion exchange to $\gamma N \to \pi^\pm \Delta$. Their calculation is in good agreement with the cross-section data[43, 48] for $|t| \leqslant m_\pi^2$. Campbell, Clark, and Horn,[49] applying "low-t theorems" to $\gamma N \to \pi^\pm \Delta$, as well as to $\gamma N \to \pi^\pm N$, set limits on the t dependence of the cross sections based on constraints that must be satisfied at the pion pole, $t = + m_\pi^2$. Given the zero-degree cross section, they were able to determine the t dependence of both the cross section

and asymmetry for $\gamma N \to \pi \Delta$ and $|t| \leqslant m_\pi^2$. Their result is similar to that obtained by Stichel and Scholz.

Polarized-photon asymmetries for these processes can be simply related to differential cross sections in the small-t region through an argument given by Harari.[50] Based on angular momentum considerations, at zero degrees $d\sigma_\perp/dt$ must equal $d\sigma_\parallel/dt$; hence either Σ or $d\sigma/dt$ must go to zero as $\theta \to 0°$. Since only pion exchange is expected to produce a strong variation in the cross section in the region $|t| \leqslant m_\pi^2$, this variation should appear in $d\sigma_\parallel/dt$, with $d\sigma_\perp/dt$ being relatively featureless. Thus, the reaction $\gamma p \to \pi^+ n$, with a factor-of-2 spike in the cross section near $0°$, should have a polarized-photon asymmetry near $+1$ at $t \sim -m_\pi^2$, while $\gamma p \to \pi^- \Delta^{++}$, which dips at $0°$ to about half of the value it has at $t \sim m_\pi^2$, should have an asymmetry near -0.5 at $t \sim -m_\pi^2$. Measurements of the polarized-photon asymmetry at small $|t|$ test the simple ideas behind Harari's argument; they do not test specific models.

In Fig. 25 we plot the $\gamma p \to \pi^+ n$ and $\gamma p \to \pi^- \Delta^{++}$ cross sections for perpendicular and parallel photons at small $|t|$. The $\gamma p \to \pi^+ n$ data clearly show that the rapid variation of the cross section at small $|t|$ is due to unnatural-parity exchange in agreement with Harari's argument. The $\gamma p \to \pi^- \Delta^{++}$ data are consistent with expectations, but the natural-parity exchange cross section does show significant variation for $|t| < m_\pi^2$. This variation is apparently associated with the dip in the cross section at $t = -0.15$ GeV^2. The $\gamma p \to \pi^+ \Delta^0$ data have larger error bars and are not plotted.

In Figs. 16 and 17 we compare our asymmetry results for single-pion production with the electric Born approximation. The agreement is good for $|t| \leqslant m_\pi^2$ in the π^+ case. The asymmetries for $\pi \Delta$ photoproduction at low $|t|$ from the minimal gauge-invariant calculation of Campbell, Clark, and Horn[49] are plotted in Fig. 20. Our measurements are in qualitative agreement, but it should be noted that the model has a constant $d\sigma_\perp/dt$, which is not in agreement with the data.

D. Vector-meson dominance

Many photo- and electroproduction processes have been discussed within the framework of vector-meson dominance. More recently these ideas have been extended to give a picture of the hadronic nature of the photon.[51] This hadronic nature plays a significant role in photon interactions, and in many ways the qualitative features of this picture are more satisfactory than the
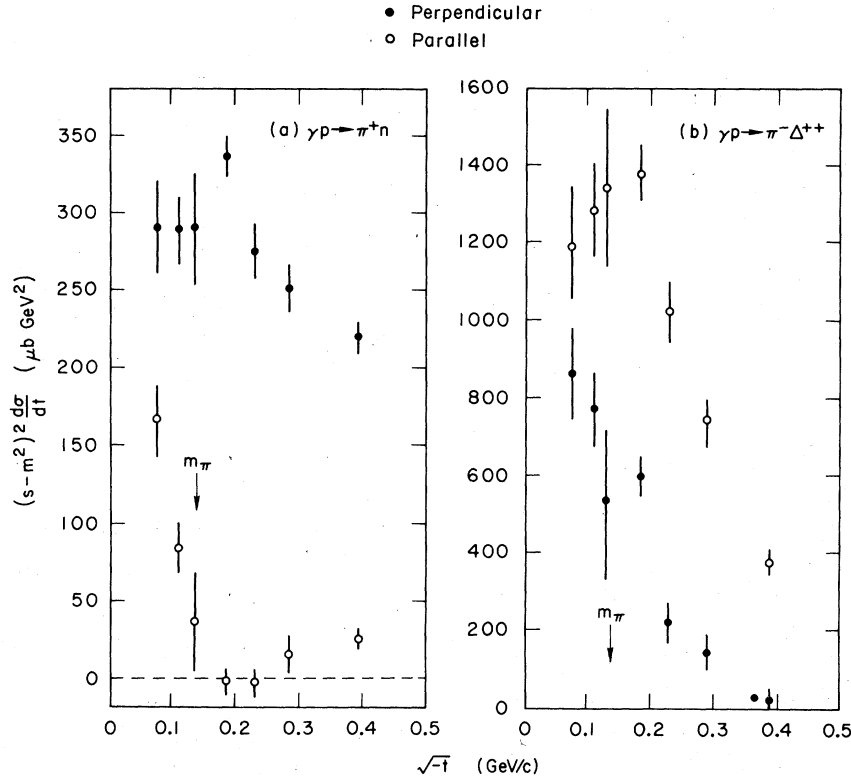
● Perpendicular
○ Parallel

FIG. 25. The small-$|t|$ cross sections for (a) single π^+ and (b) $\pi^- \Delta^{++}$ photoproduction from hydrogen.

detailed predictions of the conventional vector-dominance model.

One such straightforward detailed prediction is the comparison of the cross section and density matrix elements for $\pi^- p \rightarrow \rho^0 n$ with the cross section and asymmetry for single-pion photoproduction. For purposes of comparison, the photoproduction cross section used is

$$\frac{1}{2}\left(\frac{d\sigma}{dt}(\gamma p \rightarrow \pi^+ n) + \frac{d\sigma}{dt}(\gamma n \rightarrow \pi^- p)\right),$$

which eliminates the interference between isoscalar and isovector photons. Bulos *et al.*[52] have compared their measurements of $\pi^- p \rightarrow \rho^0 n$ at 15 GeV with the asymmetry data of Burfeindt *et al.*[9] and Geweniger *et al.*[8] They conclude that the unnatural-parity exchange cross sections are in good agreement as is the asymmetry for $|t|$ $\lesssim 2 m_\pi^2$. At almost all values of $|t|$, the natural-parity exchange cross section for photoproduction is significantly larger than that for ρ production by pions.

In Figs. 26 and 27 we compare our measurements with those of Bulos *et al.*[52] Our conclusions are the same, thereby removing whatever uncertainties may have been present due to the different energies of the ρ production and photoproduc-

tion data. Although the amount and quality of the data have improved with time, this particular failure of the vector-dominance model is essentially unchanged since the first experimental results and the early discussions by Diebold and Poirier.[53]

A comparison of the reaction $\pi^+ p \rightarrow \rho^0 \Delta^{++}$ with π-Δ photoproduction is also possible. However, this comparison involves line reversal (not merely time reversal as does the comparison for single-pion production) as well as vector dominance. Any interference terms between Regge exchanges of opposite signature change sign under line reversal.[54, 55] Taking the sum of the cross sections for the reactions $\gamma p \rightarrow \pi^- \Delta^{++}$ and $\gamma n \rightarrow \pi^+ \Delta^-$ eliminates isoscalar-isovector interference and allows comparison to the cross section and helicity-frame density matrix elements for $\pi^+ p \rightarrow \rho^0 \Delta^{++}$. The cross-section and asymmetry relationships are

$$\frac{d\sigma}{dt}(\gamma p \rightarrow \pi^- \Delta^{++}) + \frac{d\sigma}{dt}(\gamma n \rightarrow \pi^+ \Delta^-)$$

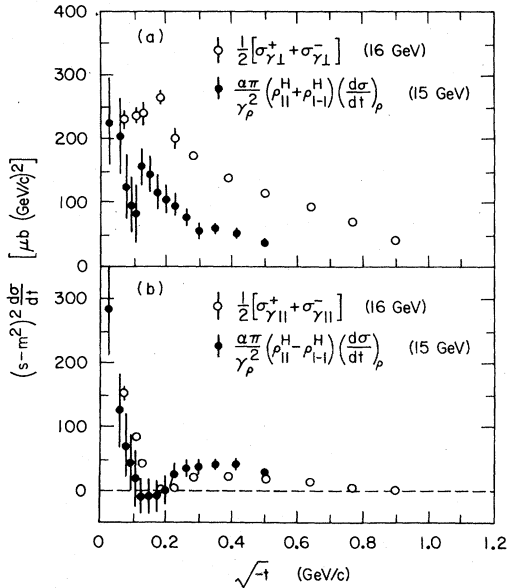$$= \frac{2\pi\alpha}{\gamma_\rho^2}\rho_{11}\frac{d\sigma}{dt}(\pi^+ p \rightarrow \rho^0 \Delta^{++})$$

and

FIG. 26.. Vector-dominance comparison of single-π photoproduction and $\pi^- p \to \rho^0 n$ (data from Ref. 52) for (a) natural-parity exchange (perpendicular photons) and (b) unnatural-parity exchange (parallel photons).

$$\Sigma = \frac{\rho_{1-1}}{\rho_{11}} \,.$$

Boyarski et al.[43] have compared their photoproduction measurements with the $\pi^+ p \to \rho^0 \Delta^{++}$ measurements of Aderholz et al.,[56] and they find that the photoproduction cross section is larger by

about a factor of 5. Cross-section measurements of the double-resonance process are difficult, and factor-of-2 disagreements at the same incident energy are not uncommon (see Fig. 1 of Ref. 57). This can explain some, but not all, of the discrepancy found by Boyarski et al.[43]

In Fig. 28, we compare our data with the 13.2-GeV cross-section measurements of Gaidos et al.,[58] measurements which these authors consider to be upper limits. In making this comparison we have multiplied both our cross sections and those of Gaidos et al.[58] by $(s - m^2)^2$. This is equivalent to scaling our 16-GeV measurements down to the 13.2-GeV incident energy of Gaidos et al.[58] The scaled cross sections have the same t dependence, but differ by a factor of approximately 1.75. A substantial part of the change from earlier results comes from using different data for the $\pi^+ p \to \rho^0 \Delta^{++}$ cross section, the different Δ normalizations, and the different energy dependence of the two processes.[48, 57, 59] This latter dependence is, of course, inconsistent with vector dominance.

The asymmetries for the two processes are in good agreement (Fig. 29). This test should be free of the systematic uncertainties in determining the cross sections. The good agreements between the t dependences of both cross sections and the asymmetries indicate that much of the previous trouble with the vector-dominance comparison for $\pi \Delta$ photoproduction may be associated with the absolute normalization of the cross sections.

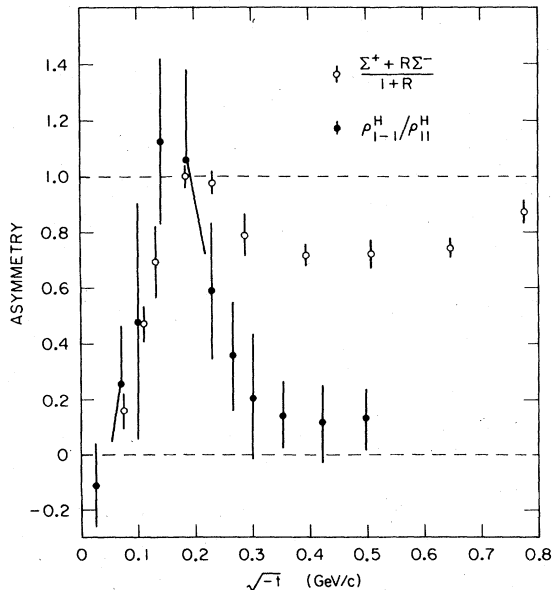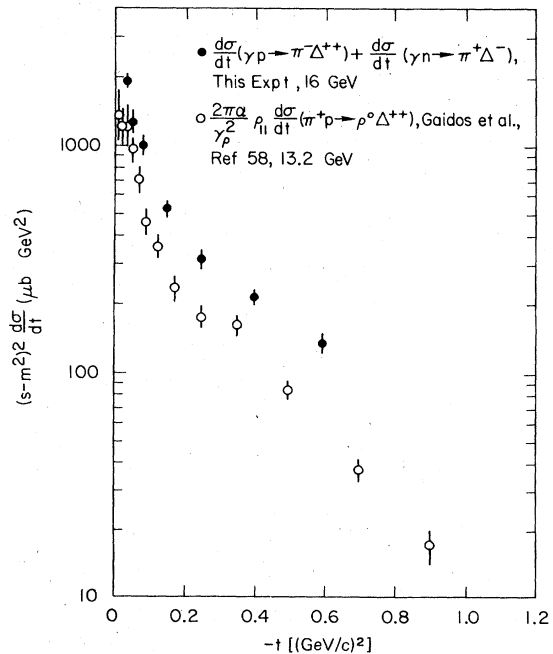
FIG. 27. The polarized-photon asymmetry from single-pion photoproduction compared with that for $\pi^- p \to \rho^0 n$. The π^- data are from Ref. 52.

FIG. 28. Comparison of the $\pi \Delta$ photoproduction cross section with that for $\pi^+ p \to \rho^0 \Delta^{++}$ (Ref. 58).

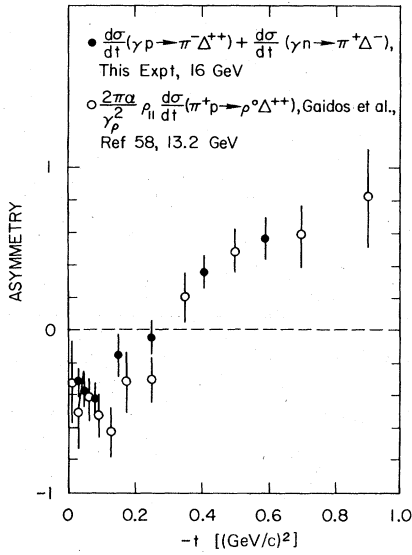FIG. 29. The $\pi^+ p \to \rho^0 \Delta^{++}$ (Ref. 58) asymmetry compared with the $\pi \Delta$ photoproduction asymmetry.

FIG. 30. The polarized-photon asymmetry for single-K^+ photoproduction from (a) hydrogen and (b) deuterium.

E. Single-K^+ photoproduction

The cross sections and asymmetries for $\gamma p \to K^+ (\Lambda, \Sigma^0)$ and $\gamma D \to K^+ (\Lambda, \Sigma^0, \Sigma^-) N_s$ are given in Table VII. The measurements from a hydrogen target agree with both the t dependence and the absolute normalization of Boyarski *et al.*[60] This normalization agreement is in contrast to the disagreement found in pion photoproduction. Many of the uncertainties in the absolute cross sections are shared by both pions and kaons, and we have not been able to understand why our kaon cross sections agree with the earlier measurements while the pion ones do not. We believe that this normalization uncertainty does not affect our asymmetry measurements.

The asymmetries are shown in Fig. 30. These measurements are consistent with one over most of the t range of the experiment; the only structure we observe is the rise of the asymmetry from
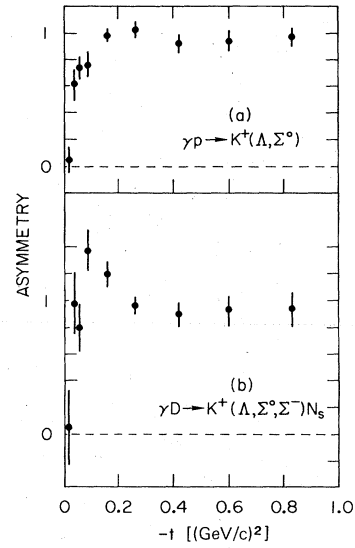
zero as $|t|$ increases. At large $|t|$ the cross sections for all measured pseudoscalar photoproduction processes are dominated by perpendicularly polarized photons. This includes the measurements presented in this paper and both π^0 and η photoproduction.[61, 62] This common feature, together with the similar t dependences and comparable magnitudes of cross sections, gives a strong hint that similar mechanisms must be important for all these reactions.

Since the asymmetries for the sum of the kaon photoproduction reactions are close to 1, and since the individual reactions have comparable cross sections, the asymmetries of the individual reactions must be close to 1. In Table VIII we present the cross sections and asymmetries for the individual processes. The difficulty in determining the contribution of individual processes to the total yield (Sec. IV B) is reflected in the

TABLE VII. Cross-section and asymmetry results for K^+-meson photoproduction from hydrogen and deuterium.

|	$\gamma p \to K^+ (\Lambda, \Sigma^0)$		$\gamma D \to K^+ (\Lambda, \Sigma^0, \Sigma^-) N_s$	
$-t$ [(GeV/c)^2]	$d\sigma/dt$ [μb/(GeV/c)^2]	Σ	$d\sigma/dt$ [μb/(GeV/c)^2]	Σ
0.015	0.0454 ± 0.0035	0.04 ± 0.11	0.0574 ± 0.0051	0.05 ± 0.28
0.037	0.0638 ± 0.0050	0.61 ± 0.12	0.104 ± 0.009	0.97 ± 0.23
0.056	0.0701 ± 0.0054	0.73 ± 0.09	0.105 ± 0.009	0.80 ± 0.18
0.086	0.0762 ± 0.0059	0.76 ± 0.10	0.127 ± 0.010	1.37 ± 0.15
0.16	0.0860 ± 0.0065	0.98 ± 0.06	0.148 ± 0.012	1.20 ± 0.09
0.26	0.0801 ± 0.0015	1.02 ± 0.07	0.135 ± 0.004	0.96 ± 0.07
0.42	0.0665 ± 0.0011	0.92 ± 0.07	0.101 ± 0.002	0.90 ± 0.09
0.60	0.0324 ± 0.0008	0.94 ± 0.09	0.0554 ± 0.0015	0.93 ± 0.11
0.83	0.0149 ± 0.0005	0.97 ± 0.08	0.0265 ± 0.0008	0.94 ± 0.12
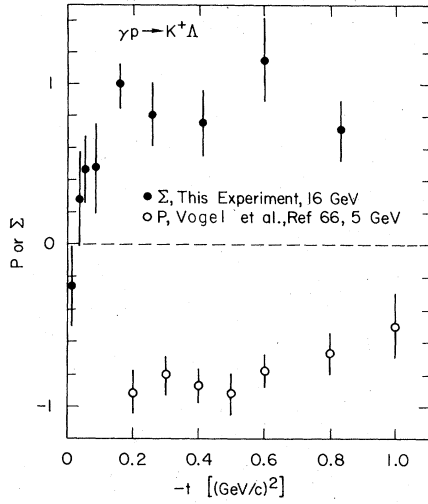
FIG. 31. The recoil-Λ-polarization measurements of Vogel et al. (Ref. 66) and the polarized-photon-asymmetry measurement for $\gamma p \to K^+\Lambda$.

large error bars. The ratios of cross sections do not compare well with those of Boyarski et al.[60, 63] This comparion is discussed in Appendix C. The asymmetry results for $\gamma p \to K^+\Lambda$ are the least uncertain; they are shown in Fig. 31. The asymmetry, which is consistent with one for $-t \geqslant 0.13$ $(\text{GeV}/c)^2$, agrees with several photoproduction models.[64, 65]

Our measurements can be combined with recoil-Λ polarization measurements at 5 GeV by Vogel et al.[66] (see Fig. 31) to give a qualitative picture of the s-channel amplitudes for K-Λ photoproduction. In terms of the s-channel amplitudes the polarized photon asymmetry is[67]

$$\Sigma = \frac{2\,\text{Re}(g_1 g_4^* + g_2 g_3^*)}{\sum_i |g_i|^2}\ ,$$

where g_1 is the helicity-nonflip amplitude, g_2 and g_3 are single-flip amplitudes and g_4 is the double-flip amplitude. For Σ close to 1, it is necessary to have $g_1 \approx g_4^*$ and $g_2 \approx g_3^*$, but nothing can be said about the relative size of the pairs of amplitudes. The recoil-Λ polarization is given by[67]

$$P = \frac{2\,\text{Im}(g_1 g_3^* - g_2 g_4^*)}{\sum_i |g_i|^2}\ .$$

With the recoil-Λ polarization close to -1, $g_3 \approx g_1^* e^{-i\pi/2}$ and $g_2 \approx g_4^* e^{i\pi/2}$, but we can tell nothing about the relative sizes of these pairs of amplitudes. Combining these two results we find that all four s-channel amplitudes must be approximately equal in magnitude with the single-flip amplitudes being 90° out of phase with the nonflip and double-flip amplitudes.

TABLE VIII. Cross-section and asymmetry results for $K^+\Lambda$ and $K^+\Sigma$ photoproduction from hydrogen and deuterium.

$-t$ [(GeV/c)²]	$\gamma p \to K^+\Lambda$		$\gamma p \to K^+\Sigma^0$		R_p [a]	$\gamma D \to K^+(\Sigma^0,\Sigma^-)N_s$		R_Σ [b]
	$d\sigma/dt$ [μb/(GeV/c)²]	Σ	$d\sigma/dt$ [μb/(GeV/c)²]	Σ		$d\sigma/dt$ [μb/(GeV/c)²]	Σ	
0.015	0.0302 ± 0.0033	-0.26 ± 0.25	0.0152 ± 0.0027	1.00 ± 0.75	0.50 ± 0.14	0.0322 ± 0.0051	0.58 ± 1.02	2.12 ± 0.50
0.037	0.0431 ± 0.0053	0.28 ± 0.30	0.0208 ± 0.0045	1.43 ± 0.79	0.48 ± 0.16	0.069 ± 0.010	1.06 ± 0.57	3.31 ± 0.86
0.056	0.0491 ± 0.0054	0.47 ± 0.21	0.0210 ± 0.0044	1.68 ± 0.76	0.42 ± 0.13	0.073 ± 0.010	1.14 ± 0.50	3.47 ± 0.87
0.086	0.0432 ± 0.0055	0.47 ± 0.28	0.0330 ± 0.0055	1.11 ± 0.50	0.76 ± 0.22	0.080 ± 0.010	0.09 ± 0.44	2.41 ± 0.50
0.16	0.0499 ± 0.0043	0.99 ± 0.14	0.0362 ± 0.0038	0.98 ± 0.26	0.72 ± 0.14	0.095 ± 0.011	1.26 ± 0.29	2.63 ± 0.40
0.26	0.0507 ± 0.0035	0.81 ± 0.20	0.0294 ± 0.0041	1.53 ± 0.48	0.58 ± 0.12	0.0868 ± 0.0055	1.04 ± 0.20	2.95 ± 0.45
0.42	0.0314 ± 0.0025	0.76 ± 0.21	0.0230 ± 0.0030	1.26 ± 0.40	0.73 ± 0.15	0.0653 ± 0.0061	0.88 ± 0.27	2.84 ± 0.45
0.60	0.0194 ± 0.0019	1.15 ± 0.25	0.0130 ± 0.0023	0.45 ± 0.51	0.66 ± 0.18	0.0373 ± 0.0049	1.13 ± 0.34	2.88 ± 0.63
0.83	0.0098 ± 0.0008	0.72 ± 0.19	0.0051 ± 0.0009	1.83 ± 0.57	0.52 ± 0.13	0.0160 ± 0.0032	0.97 ± 0.47	3.11 ± 0.84

[a] $R_p \equiv \dfrac{d\sigma/dt(\gamma p \to K^+\Sigma^0)}{d\sigma/dt(\gamma p \to K^+\Lambda)}$.

[b] $R_\Sigma \equiv \dfrac{d\sigma/dt(\gamma D \to K^+(\Sigma^0,\Sigma^-)N_s)}{d\sigma/dt(\gamma p \to K^+\Sigma^0)}$.

VI. CONCLUSIONS

From our study of the polarized-photon asymmetries in pseudoscalar-meson photoproduction, we conclude the following:

(1) All the reactions we studied are dominated by natural-parity exchange at large $|t|$.

(2) The energy dependence for single-pion photoproduction with parallel polarized photons is consistent with that expected from a pion Regge trajectory.

(3) There is significant interference between natural-parity exchanges of opposite G parity in both single-pion and π-Δ photoproduction.

(4) There is evidence for some interference between unnatural-parity exchanges of opposite G parity in π-Δ photoproduction, but no evidence exists in single-pion photoproduction.

(5) Although we observe a dip in the natural-parity-exchange cross section for $\gamma p \to \pi^- \Delta^{++}$ at $t = -0.15$ GeV^2, it seems unlikely that this channel is dominated by a single s-channel amplitude.

(6) The asymmetries at small $|t|$ for single-pion and π-Δ photoproduction are well described by qualitative arguments relating them to the cross sections.

(7) Simple vector-meson dominance describes the unnatural-parity single-pion photoproduction cross sections, and the asymmetry for this process at low t. It fails completely for the natural-parity cross section. It does describe the asymmetry for π-Δ photoproduction, and the shape, but not the magnitude, of the cross section.

(8) For $|t| > m_K^2$ the K^+ asymmetries are consistent with 1.

(9) For $K^+\Lambda$ photoproduction the asymmetry is close to $+1$ and the recoil Λ polarization to -1, which implies all four s-channel amplitudes are of comparable magnitude.

(10) The fact that all pseudoscalar-meson photoproduction processes observed to date show dominance of natural-parity exchange, similar t dependences, $1/k^2$ scaling, and cross sections of comparable magnitude, strongly suggests a common underlying mechanism for these reactions.

APPENDIX A: MISSING MASS SQUARED IN AN EXPERIMENT WITH A FOCUSING SPECTROMETER AND A BREMSSTRAHLUNG BEAM

The intersection of a particle trajectory with the momentum and θ focal planes of the spectrometer measures both δ, the percentage deviation of the momentum from the central momentum p_0, and $\theta - \theta_0$, the deviation of the horizontal production angle from θ_0, the central angle of the spectrometer. For conceptual purposes, these focal planes can be combined into a single δ-θ plane, shown in Fig. 32.

Given the masses of the target and detected particles, m_T and m_D, respectively, and assuming a photon energy k, the missing mass squared M^2 of the undetected particle(s) is given by

$$M^2 = m_T^2 + m_D^2 - (2m_T p_0/\beta)(1 + \delta/100)$$
$$+ 2k[m_T - p_0(1 + \delta/100)(1/\beta - \cos\theta \cos\Phi)] .$$

In this equation β is the normalized velocity of m_D, taken to be a constant over the spectrometer acceptance, and Φ is the vertical production angle. Thus lines of constant missing mass squared have a slope in the δ-θ plane of

$$\left.\frac{\partial\delta}{\partial\theta}\right|_{M^2=\text{const}} = \frac{-100k(1 + \delta/100)\sin\theta \cos\Phi}{m_T/\beta + k(1/\beta - \cos\theta \cos\Phi)} .$$

This slope is independent of p_0, and the dependence on δ, θ, and Φ is sufficiently weak that within the spectrometer acceptance the slope may be considered independent of these variables.

In the present experiment the spectrometer accepted only particles produced by photons of en-
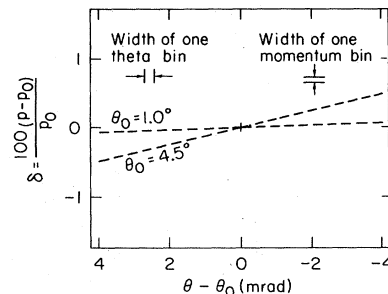
FIG. 32. The δ-θ plane. Lines of constant missing mass squared$=m_p^2$ are shown for two values of the central spectrometer angle.

ergies very near the bremsstrahlung end point. Thus one can divide the δ-θ plane into bins of constant missing mass squared which are essentially independent of k. At a fixed photon energy, the principal variation in the cross section at fixed p_0 is due to the change in missing mass with angle. By using bins of constant missing mass squared rather than bins of constant momentum, this variation of cross section within a bin is avoided. In labeling a bin, we have used the convention $K = E_0 - 0.05$ GeV, where E_0 is the end-point energy.

APPENDIX B: PARAMETRIZATIONS USED IN FITTING THE MOMENTUM DISTRIBUTIONS

1. Photon spectrum

The photon-beam spectrum employed in the fits was determined by multiplying the calculated bremsstrahlung spectrum[17] from an amorphous radiator by the experimentally determined attenuation function.[15] This attenuation function, which accounted for the spectrum degradation by the graphite absorber, is discussed in Sec. II A. In fitting data from the deuterium target, the photon-beam spectrum was "smeared" to account for the Fermi motion of the target nucleons. The Hulthén[68] wave function for the deuteron was used for this modification. In the remainder of this appendix, we denote the photon-beam spectrum by $n(k)$. The normalization is such that the number of photons per equivalent quantum between k and $k + dk$ is $n(k)dk$.

2. The reactions $\gamma N \to \pi N$, $\gamma N \to K\Lambda$, and $\gamma N \to K\Sigma$

As these reactions all have stable undetected recoil baryons, for any given detected particle momentum p, and production angle θ, only photons of a particular energy, k_0, can produce a yield. k_0 is given by

$$k_0 = \frac{m_R^2 - m_T^2 - m_D^2 + 2m_T E}{2(m_T - E + p\cos\theta)},$$

where m_R, m_T, and m_D are the masses of recoil, target, and detected particles, respectively, and E is the laboratory energy of the detected particle. The number of photons per equivalent quantum which can contribute to the yield is

$$n(k_0)dk = n(k_0)\frac{\partial k}{\partial p}dp.$$

We evaluate the derivative $\partial k/\partial p$ at the normal photon energy K (=16 GeV). The cross section per equivalent quantum is given by

$$\frac{1}{Q}\frac{d^2\sigma}{d\Omega dp/p} = p\frac{\partial k}{\partial p}n(k_0)\frac{d\sigma(p)}{d\Omega}.$$

At high energy, the cross sections for pseudoscalar-meson photoproduction reactions differential in the laboratory solid angle are, to an excellent approximation, independent of the photon energy at a fixed t. Thus, at a fixed laboratory angle, the cross section depends on momentum only through the momentum dependence of t. We therefore use the approximation

$$\frac{d\sigma}{d\Omega}(p) = \frac{d\sigma}{d\Omega}(p_0)\exp\left(\frac{dt}{dp}\bigg|_{p_0}(p - p_0)A\right),$$

where p_0 is the detected particle momentum produced by a 16-GeV photon. The parameter A, the t-dependent logarithmic slope of the π-N, K-Λ, or K-Σ cross section, is taken from the results of Boyarski et al.[35,60] $(d\sigma/d\Omega)(p_0)$, the single unknown, is the cross section for photoproduction by 16-GeV photons. Combining these relations, we obtain

$$\frac{1}{Q}\frac{d^2\sigma}{d\Omega dp/p} = p\frac{\partial k}{\partial p}n(k_0)$$

$$\times \exp\left(\frac{dt}{dp}\bigg|_{p_0}(p - p_0)A\right)\frac{d\sigma}{d\Omega}(p_0).$$

3. The reactions $\gamma N \to \pi\Delta(1236)$

For this case, where the recoil mass is not sharp but has a broad resonance shape, the differential cross section for a photon of energy k to produce a $\pi\Delta$ final state with a Δ of mass m is

$$\frac{d\sigma}{d\Omega}(k,m) = \frac{d\sigma_0}{d\Omega}(k,m)F_{BW}(m)dm^2$$

$$= \frac{d\sigma_0}{d\Omega}(k,m)\left[\frac{1}{\pi}\frac{m_0\Gamma(m)}{(m_0^2 - m^2)^2 + m_0^2\Gamma^2(m)}\right]dm^2,$$

where m_0 is the central mass of the Δ(=1.236 GeV/c^2), $\Gamma(m)$ is the mass-dependent width, and $d\sigma_0/d\Omega$ (k,m) is the "stable-particle" production cross section. We use the CERN 3-3 phase shifts[69] to calculate this width[70]:

$$\Gamma(m) = \tan\delta_{33}(m_0^2 - m^2)/m_0.$$

We assume the only mass and energy dependence of $d\sigma_0/d\Omega$ is due to the dependence of the π-Δ two-body phase space on mass and energy and to the variation of t with these quantities. Thus, we have

$$\frac{d\sigma_0}{d\Omega}(k,m) = \frac{d\sigma_0}{d\Omega}(K,m_0)\frac{\text{phase space}(k,m)}{\text{phase space}(K,m_0)}$$

$$\times \exp[A_{\pi\Delta}(t(k,m) - t(K,m_0))],$$

where $A_{\pi\Delta}$ is the t-dependent logarithmic slope of the $\pi\Delta$ cross section and K is the nominal photon energy, 16 GeV. We take $A_{\pi\Delta}$ from the results of Boyarski et al.[43] Denoting the phase-space ratio as $R_{PS}(m,k)$, we obtain

$$\frac{d^2\sigma}{Qd\Omega\, dp/p} = p\,\frac{d\sigma_0}{d\Omega}(K,m_0)\int_{k_{\min}}^{E_0}\left[n(k)R_{\mathrm{PS}}(m,k)\,\exp[A_{\pi\Delta}(t(k,m)-t(K,m_0))]F_{\mathrm{BW}}(m)\left|\frac{dm^2}{dp}\right|\right]dk,$$

where $k_{\min}$ is the lowest photon energy which can contribute to the yield. Again, the single unknown is the cross section for π-Δ production with a Δ mass m_0 by photons of energy K.

Note that our definition of the cross section is analogous to that suggested by Spital and Yennie[71] for ρ-meson production. The cross sections we quote are larger than those of Boyarski *et al.*[43,48] and Bingham *et al.*[72] by constant factors of 1.13 and 1.22, respectively. These differences arise because these authors have chosen to normalize the Breit-Wigner forms they use, something we have not done.

4. The reactions $\gamma N \to \pi N^*(1520)$

To obtain acceptable fits to our pion momentum spectra, it was found necessary to include π-$N^*(1520)$ production in those channels where it is allowed by isospin conservation. We have parametrized the cross section section for this reaction in the same way as for π-N production, using the general form for the mass-dependent width for baryon resonances.[70] The uncertainties are sufficiently great that we quote no results for this reaction.

5. Pions from ρ decay

The complete ρ decay distribution is given in Refs. 13 and 14. We have approximated the helicity-frame density matrix elements as

$$\rho_{00}^0 = \mathrm{Re}\rho_{10}^0 = \rho_{1-1}^0 = \rho_{11}^1$$
$$= \rho_{00}^1 = \mathrm{Re}\rho_{10}^1 = \mathrm{Im}\rho_{10}^2 = 0,$$

and

$$\rho_{1-1}^1 = -\mathrm{Im}\rho_{1-1}^2 = 0.5.$$

The resulting decay distribution is

$$W(\cos\theta,\phi,\Phi_\gamma) = \frac{3}{8\pi}\sin^2\theta[1 - P\cos2(\phi - \Phi_\gamma)],$$

where the angles are defined in Fig. 33 and P is the degree of linear polarization.

The only variable fixed by the experiment is one pion momentum. The distributions of photon energy and ρ-meson mass are also known. We express other quantities in terms of these three variables and, for convenience, work in the γ-p center of mass. Variables in this frame are denoted with an asterisk. The relation between the ρ mass $m_{\pi\pi}$, ρ momentum p_ρ^*, and photon energy k^* is

$$k^* = \frac{2p_\rho^{*2} + m_{\pi\pi}^2 + 2[(p_\rho^{*2} + m_{\pi\pi}^2)(p_\rho^{*2} + m_p^2)]^{1/2}}{2[(p_\rho^{*2} + m_{\pi\pi}^2)^{1/2} + (p_\rho^{*2} + m_p^2)^{1/2}]},$$

where m_p is the proton mass. For a given ρ momentum and mass, the pion momentum determines the decay angle θ_d^* by

$$\cos\theta_d^* = (2E_\rho^* E_\pi^* - m_{\pi\pi}^2)/2p_\rho^* p_\pi^*.$$

ρ mesons with momentum vectors lying on the surface of a cone of half angle θ_d^* with an axis along the pion momentum can decay into pions of momentum p_π^*. The angular range of the detected pions is determined by the pion momentum bite by

$$d(\cos\theta_d^*) = dp_\pi^* \frac{d(\cos\theta_d^*)}{dp_\pi^*}.$$

The $\pi\pi$ production cross section is

$$\frac{d^2\sigma}{dt\,dm_{\pi\pi}^2} = \frac{d\sigma_0(m_{\pi\pi}^2)}{dt} F_{\mathrm{BW}},$$

where σ_0 is the stable-particle production cross section and F_{BW} is the Breit-Wigner form for the ρ:

$$F_{\mathrm{BW}} = \frac{1}{\pi}\frac{m_\rho\Gamma(m_{\pi\pi})}{(m_{\pi\pi}^2 - m_\rho^2)^2 + m_\rho^2\Gamma^2(m_{\pi\pi})}.$$

The mass-dependent width is taken from Jackson[70]

$$\Gamma(m_{\pi\pi}) = \Gamma_\rho\left(\frac{Q(m_{\pi\pi})}{Q(m_\rho)}\right)^3\left(\frac{2Q^2(m_\rho)}{Q^2(m_\rho) + Q^2(m_{\pi\pi})}\right),$$

where

$$Q(m) = (m^2 - 4m_\pi^2)^{1/2}/2$$

is the π momentum in the ρ rest frame. We have used $\Gamma_\rho = 0.125$ GeV/c^2 and $m_\rho = 0.765$ GeV/c^2.
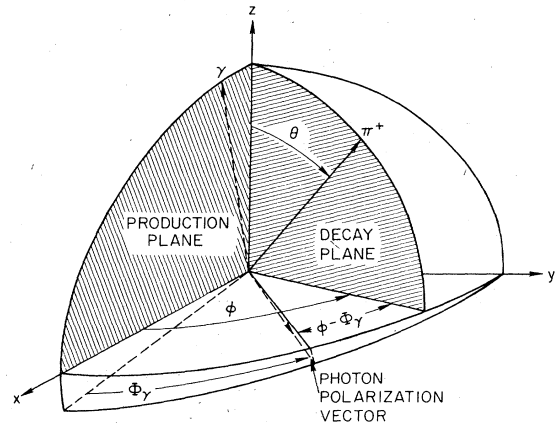
We assume that the stable-particle cross sec-

FIG. 33. The angles used in the ρ^0 decay parametrization.

tion depends on the photon energy and ρ mass through the dependence of t and the two-body phase space [for $\gamma p \to p(\pi\pi)$] on these factors, and on the ρ mass through a Ross-Stodolsky factor[73]:

$$\frac{d\sigma_0(m_{\pi\pi}{}^2)}{dt} = A e^{bt} R_{\mathrm{PS}} \left(\frac{m_\rho}{m_{\pi\pi}}\right)^{n(t)}$$

where A is for 16-GeV photons, b and $n(t) = \alpha + \beta t$ are given in Refs. 13 and 14, and R_{PS} is the phase-space ratio

$$R_{\mathrm{PS}} = \left(\frac{\lambda(s, m_{\pi\pi}{}^2, m_\rho{}^2)}{\lambda(s_0, m_\rho{}^2, m_\rho{}^2)}\right)^{1/2} \frac{s_0}{s}.$$

In this equation s_0 is the square of the center-of-mass energy for the reaction when a photon energy of 16 GeV is assumed. Also,

$$\lambda(a,b,c) = a^2 + b^2 + c^2 - 2ab - 2ac - 2bc.$$

The integration over the azimuthal angle of the cone can be done analytically, and the resulting center-of-mass cross section is transformed into the laboratory to be integrated over the photon spectrum and the ρ mass shape. The only free parameter is A. Despite the extensive ρ photoproduction data available, we have allowed A to be a free parameter, as the background to the $\pi\Delta$ reaction is from a ρ-mass region where data are unavailable.

APPENDIX C: K^+ PHOTOPRODUCTION. CROSS-SECTION RATIOS AND EXOTIC EXCHANGES

In Table VIII we present the cross-section and asymmetry results for the processes $\gamma p \to K^+\Lambda$, $\gamma p \to K^+\Sigma^0$, and $\gamma D \to K^+(\Sigma^0, \Sigma^-)$. To determine these results it is necessary to determine the contribution of each process to the step in the yield. A look at Fig. 13 should convince the reader of the difficulty of the procedure. The resultant errors are large and highly correlated, and the possibility of additional errors in the data and fitting procedures cannot be eliminated. The determination of the results for each of the three processes has different problems.

For $\gamma p \to K^+\Lambda$ the asymmetry is determined reasonably well. With our known momentum resolution the highest momentum portion of the K^+ yield must be due to $K^+\Lambda$ production. The $K^+\Lambda$ asymmetry is determined by this portion of the yield. The $K^+\Lambda$ cross section is more difficult to determine because one in effect uses the momentum resolution and the initial rate of rise of the yield to
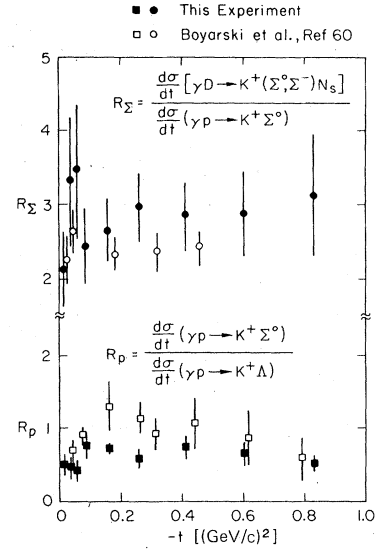

FIG. 34. The Σ^0/Λ ratio for single-K^+ photoproduction from hydrogen, compared with the results of Ref. 60, and the deuterium-to-hydrogen ratio for Σ photoproduction compared with the results of Ref. 63.

measure the cross section. Small effects such as magnet hysteresis or non-Gaussian resolutions could significantly affect the results.

Both the cross section and asymmetry for $\gamma p \to K^+\Sigma^0$ are affected by any error in the $K^+\Lambda$ quantities. The reason is that $K^+\Lambda$ is contributing to the yield at all momenta which are being used to measure the $K^+\Sigma^0$ cross section and asymmetry. The ratio of $K^+\Sigma^0$ to $K^+\Lambda$ cross sections is shown in Fig. 34. We find a generally lower result than Boyarski et al.[60]

The results for $\gamma D \to K^+(\Sigma^0, \Sigma^-)$ suffer from the same problem; they are very sensitive to any error in the $\gamma p \to K^+\Lambda$ measurements. In Fig. 34 we compare our results for the ratio R_Σ of $\gamma D \to K^+(\Sigma^0, \Sigma^-)$ to $\gamma p \to K^+\Sigma^0$ with measurements at 11 GeV.[63] At 11 GeV where the Λ-Σ separation is easier, this ratio averaged over all data points is 2.37 ± 0.11. This is not consistent with the value of 3 expected for pure isotopic spin $\frac{1}{2}$ in the t channel.

Our ratio has an average value of 2.73 ± 0.18 which is consistent with 3. We see no evidence for exotic exchanges in K^+ photoproduction. However, we do not feel this result is in disagreement with the result at 11 GeV because of the difficulty in measuring this ratio from our data.

*Present address: SRI International, Menlo Park, Calif. 94025.

†Present address: University of Washington, Seattle, Wash. 98195.

‡Present address: University of Illinois, Urbana, Ill. 61801.

§Present address: Cornell University, Ithaca, N. Y. 14853.

[1] P. Stichel, Z. Phys. 180, 170 (1964).

[2] J. P. Ader, M. Capdeville, G. Cohen-Tannoudji, and Ph. Salin, Nuovo Cimento 56A, 952 (1968); F. Ravndal, Phys. Rev. D 2, 1278 (1970).

[3] N. Cabibbo, G. Da Prato, G. De Franceschi, and U. Mosco, Phys. Rev. Lett. 9, 270 (1962); N. Cabibbo *et al.*, Nuovo Cimento 27, 979 (1963).

[4] C. Berger, G. McClellan, N. Mistry, H. Ogren, B. Sandler, J. Swartz, P. Walstrom, R. L. Anderson, D. Gustavson, J. Johnson, I. Overman, R. Talman, B. H. Wiik, D. Worcester, and A. Moore, Phys. Rev. Lett. 25, 1366 (1970).

[5] D. J. Sherden, R. H. Siemann, C. K. Sinclair, D. J. Quinn, J. P. Rutherfoord, and M. A. Shupe, Phys. Rev. Lett. 30, 1230 (1973); 31, 667(E) (1973).

[6] D. J. Quinn, J. P. Rutherfoord, M. A. Shupe, D. J. Sherden, R. H. Siemann, and C. K. Sinclair, Phys. Rev. Lett. 34, 543 (1975).

[7] Z. Bar-Yam, J. De Pagter, J. Dowd, W. Kern, D. Luckey, and L. S. Osborne, Phys. Rev. Lett. 25, 1053 (1970).

[8] Chr. Geweniger, P. Heide, U. Kötz, R. A. Lewis, P. Schmüser, H. J. Skronn, H. Wahl, and K. Wegener, Phys. Lett. 29B, 41 (1969).

[9] H. Burfeindt, G. Buschhorn, C. Geweniger, P. Heide, R. Kotthaus, H. Wahl, and K. Wegener, Phys. Lett. 33B, 509 (1970).

[10] R. F. Schwitters, J. Leong, D. Luckey, L. S. Osborne, A. M. Boyarski, S. D. Ecklund, R. Siemann, and B. Richter, Phys. Rev. Lett. 27, 120 (1971).

[11] Z. Bar-Yam, J. De Pagter, J. Dowd, and W. Kern, Phys. Rev. Lett. 24, 1078 (1970).

[12] H. Burfeindt, G. Buschhorn, C. Geweniger, R. Kotthaus, H. J Skronn, H. Wahl, and K. Wegener, Nucl. Phys. B59, 87 (1973).

[13] J. Ballam, G. B. Chadwick, R. Gearhart, Z. G. T. Guiragossian, J. J. Murray, P. Seyboth, C. K. Sinclair, I. O. Skillicorn, H. Spitzer, G. Wolf, H. H. Bingham, W. B. Fretter, K. C. Moffeit, W. J. Podolsky, M. S. Rabin, A. H. Rosenfeld, R. Windmolders, and R. H. Milburn, Phys. Rev. D 5, 545 (1972).

[14] J. Ballam, G. B. Chadwick, Y. Eisenberg, E. Kogan, K. C. Moffeit, P. Seyboth, I. O. Skillicorn, H. Spitzer, G. Wolf, H. H. Bingham, W. B. Fretter, W. J. Podolsky, M. S. Rabin, A. H. Rosenfeld, and G. Smadja, Phys. Rev. D 7, 3150 (1973).

[15] R. L. Eisele, D. J. Sherden, R. H. Siemann, C. K. Sinclair, D. J. Quinn, J. P. Rutherfoord, and M. A. Shupe, Nucl. Instrum. Methods 113, 489 (1973).

[16] G. E. Fischer and Y. Murata, Nucl. Instrum. Methods 78, 25 (1970).

[17] R. A. Early, SLAC Report No. SLAC-TN-66-15, 1966 (unpublished).

[18] SLAC Users Handbook, 1971 (unpublished); p. D. 3–7; A. M. Boyarski, D. H. Coward, S. Ecklund, B. Richter, D. Sherden, R. Siemann, and C. Sinclair, Phys. Rev. Lett. 26, 1600 (1971).

[19] R. S. Larsen and D. Horelick, SLAC Report No. SLAC-PUB-559, 1969 (unpublished); or in the Proceedings of the Symposium on Beam Intensity Measurement, Daresbury, 1968 (unpublished), pp. 260–279.

[20] D. Yount, Nucl. Instrum. Methods 52, 1 (1967).

[21] R. L. Anderson, Nucl. Instrum. Methods 70, 87 (1969).

[22] A. M. Boyarski, D. H. Coward, S. D. Ecklund, B. Richter, D. J. Sherden, R. H. Siemann, and C. K. Sinclair, Phys. Rev. D 14, 1733 (1976).

[23] SLAC Users Handbook, 1971 (unpublished), p. D.3-5.

[24] A. M. Boyarski, private communication.

[25] R. F. Schwitters, Ph. D. thesis, MIT, 1971 (unpublished).

[26] The Jacobians for single pion or single K^+ photoproduction are evaluated at 16.00-GeV incident energy. Treating these as constants is a good approximation in the momentum range we cover. In this paper, k refers to a general photon energy, and K to the specific energy $E_0 - 0.05$ GeV.

[27] E. Taylor, private communication.

[28] We use the same stringent region as Boyarski *et al.* Their calculation of the acceptance of this region was used in Refs. 35, 36, 43, 48, 60, and 63.

[29] We have used the program SOLVE written by C. Moore.

[30] References 13 and 14 and K. Moffeit, private communication.

[31] K. C. Moffeit, J. Ballam, G. B. Chadwick, M. Della-Negra, R. Gearhart, J. J. Murray, P. Seyboth, C. K. Sinclair, I. O. Skillicorn, H. Spitzer, G. Wolf, H. H. Bingham, W. B. Fretter, W. J. Podolsky, M. S. Rabin, A. H. Rosenfeld, R. Windmolders, G. P. Yost, and R. H. Milburn, Phys. Rev. D 5, 1603 (1972).

[32] S. D. Drell, Phys. Rev. Lett. 5, 278 (1960).

[33] F. von Holtey, in *Proceedings of the Symposium on Meson Photo- and Electroproduction at Low and Intermediate Energies, Bonn, 1970* (Springer, New York, 1971).

[34] W. S. C. Williams, *An Introduction to Elementary Particles* (Academic, New York, 1971), 2nd edition, p. 444.

[35] A. M. Boyarski, F. Bulos, W. Busza, R. Diebold, S. D. Ecklund, G. E. Fischer, J. R. Rees, and B. Richter, Phys. Rev. Lett. 20, 300 (1968).

[36] A. M. Boyarski, R. Diebold, S. D. Ecklund, G. E. Fischer, Y. Murata, B. Richter, and W. S. C. Williams, Phys. Rev. Lett. 21, 1767 (1968).

[37] D. I. Julius, Nucl. Phys. B40, 409 (1972).

[38] B. H. Kellett, Nucl. Phys. B25, 205 (1970).

[39] Z. Bar-Yam, J. de Pagter, M. M. Hoenig, W. Kern, D. Luckey, and L. S. Osborne, Phys. Rev. Lett. 19, 40 (1967).

[40] P. Heide, U. Kötz, R. A. Lewis, P. Schmüser, H. J. Skronn, and H. Wahl, Phys. Rev. Lett. 21, 248 (1968).

[41] The identification of the A_3 as $J^P = 2^-$ makes it a strong candidate as the first recurrence of the pion. G. Ascoli, D. V. Brockway, L. Eisenstein, J. D. Hansen, M. L. Ioffredo, U. E. Kruse, T. F. Johnston, A. W. Key, J. D. Prentice, T. S. Yoon, C. Caso, G. Tomasini, P. von Handel, P. Schilling, G. Costa, S. Ratti, L. Mosca, W. C. Harrison, D. Heyda, W. H. Johnson, Jr., J. K. Kim, M. E. Law, J. E. Mueller, B. M. Salzberg, L. K. Sisterson, H. Grassler, W. D. Nowak, M. Rost, G. T. Jones, W. Kittel, S. Brandt, P. H. Smith, W. D. Shephard, N. N. Biswas, N. M. Casca, V. P. Kenney, W. B. Madden, A. R. Erwin,

R. Morse, B. Y. Oh, W. Robertson, and W. D. Walker, Phys. Rev. D **7**, 669 (1973).

[42]R. C. E. Devenish, W. J. Leigh, and D. H. Lyth, Nuovo Cimento **1A**, 475 (1971).

[43]A. M. Boyarski, R. Diebold, S. D. Ecklund, G. E. Fischer, Y. Murata, B. Richter, and M. Sands, Phys. Rev. Lett. **25**, 695 (1970); **25**, 1148(E) (1970).

[44]Y. Eisenberg, B. Haber, U. Karshon, J. Mikenberg, S. Pitluck, E. E. Ronat, A. Shapira, and G. Yekutieli, Phys. Lett. **48B**, 354 (1974).

[45]G. R. Goldstein and J. F. Owens, Nucl. Phys. **B71**, 461 (1974).

[46]R. B. Clark, Phys. Rev. D **18**, 1444 (1978).

[47]P. Stichel and M. Scholz, Nuovo Cimento **34**, 1381 (1964).

[48]A. M. Boyarski, R. Diebold, S. D. Ecklund, G. E. Fischer, Y. Murata, B. Richter, and W. S. C. Williams, Phys. Rev. Lett. **22**, 148 (1969).

[49]J. A. Campbell, R. B. Clark, and D. Horn, Phys. Rev. D **2**, 217 (1970).

[50]H. Harari, in the *Proceedings of the Fourth International Symposium on Electron and Photon Interactions at High Energies, Liverpool*, 1969, edited by D. W. Braben and R. E. Rand (Daresbury Nuclear Physics Laboratory, Daresbury, Lancashire, England, 1970).

[51]T. H. Bauer, R. D. Spital, D. R. Yennie, and F. M. Pipkin, Rev. Mod. Phys. **50**, 261 (1978).

[52]F. Bulos, R. K. Carnegie, G. E. Fischer, E. E. Kluge, D. W. G. S. Leith, H. L. Lynch, B. Ratcliff, B. Richter, H. H. Williams, and S. H. Williams, Phys. Rev. Lett. **26**, 1457 (1971).

[53]R. Diebold and J. Poirier, Phys. Rev. Lett. **22**, 255 (1969).

[54]E. Gotsman, Lett. Nuovo Cimento **2**, 563 (1969).

[55]F. Gilman, Phys. Lett. **29B**, 673 (1969).

[56]M. Aderholz, M. Deutschmann, E. Keppel, G. Kraus, H. Weber, C. Grote, H. H. Kaufmann, S. Novak, M. Walter, H. Bottcher, T. Byer, V. T. Cocconi, P. F. Dalpiaz, J. D. Hansen, G. Kellner, W. Kittel, M. Markytan, A. Mihul, D. R. O. Morrison, and H. T. Tøfte, Nucl. Phys. **B8**, 45 (1968).

[57]R. O. Maddock, G. F. Pinter, D. Evans, C. Caso, F. Conte, D. Teodoro, G. Tomasini, H. Fesefeld, P. von Handel, H. Nagel, P. K. Schilling, G. Cecchet, L. Mandelli, S. Ratti, L. Tallone Lombardi, M. Chaumet, A. Daudin, M. Faccini, M. A. Jabiol, J. F. Lefur, C. Lewin, and J. Mallet, Nuovo Cimento **5A**, 433

(1971).

[58]J. A. Gaidos, A. A. Hirata, R. J. DeBonte, T. A. Mulera, G. Thompson, and R. B. Willmann, Nucl. Phys. **B72**, 253 (1974).

[59]N. N. Biswas, N. M. Cason, M. S. Farber, J. A. Helland, M. J. Hones, V. P. Kenney, J. T. McGahan, J. A. Poirier, J. T. Powers, O. R. Sander, and W. D. Shephard, Phys. Rev. D **2**, 2529 (1970).

[60]A. M. Boyarski, F. Bulos, W. Busza, R. Diebold, S. D. Ecklund, G. E. Fischer, Y. Murata, J. R. Rees, B. Richter, and W. S. C. Williams, Phys. Rev. Lett. **22**, 1131 (1969).

[61]R. L. Anderson, D. B. Gustavson, J. R. Johnson, I. D. Overman, D. M. Ritson, B. H. Wiik, and D. Worcester, Phys. Rev. D **4**, 1937 (1971).

[62]P. J. Bussey, C. Raine, J. G. Rutherglen, P. S. L. Booth, L. J. Carroll, P. R. Daniel, A. W. Edwards, C. J. Hardwick, J. R. Holt, J. N. Jackson, J. Norem, W. H. Range, W. Galbraith, V. H. Rajaratnam, C. Sutton, M. C. Thorne, and P. Waller, Phys. Lett. **61B**, 479 (1976).

[63]A. M. Boyarski, R. Diebold, S. D. Ecklund, G. E. Fischer, Y. Murata, B. Richter, and M. Sands, Phys. Lett. **34B**, 547 (1971).

[64]G. R. Goldstein, J. F. Owens, and J. P. Rutherfoord, Nucl. Phys. **B53**, 197 (1973).

[65]N. Levy, W. Majerotto, and B. J. Read, Nucl. Phys. **B55**, 493 (1973).

[66]G. Vogel, H. Burfeindt, G. Buschhorn, P. Heide, U. Kötz, K.-H. Mess, R. Schmüser, B. Sonne, and B. H. Wiik, Phys. Lett. **40B**, 513 (1972).

[67]J. D. Jackson and C. Quigg, Nucl. Phys. **B22**, 301 (1970).

[68]L. Hulthén, Phys. Rev. **61**, 671 (1942).

[69]A. Donnachie, R. G. Kirsopp, and C. Lovelace, Phys. Lett. **26B**, 161 (1968).

[70]J. D. Jackson, Nuovo Cimento **34**, 1644 (1964).

[71]R. Spital and D. R. Yennie, Phys. Rev. D **9**, 126 (1974).

[72]H. H. Bingham, W. B. Fretter, K. C. Moffeit, W. J. Podolsky, M. S. Rabin, A. H. Rosenfeld, R. Windmolders, J. Ballam, G. B. Chadwick, R. Gearhart, Z. G. T. Guiragossian, M. Menke, J. J. Murray, P. Seyboth, A. Shapira, C. K. Sinclair, I. O. Skillicorn, G. Wolf, and R. H. Milburn, Phys. Rev. Lett. **25**, 1223 (1970).

[73]M. Ross and L. Stodolsky, Phys. Rev. **149**, 1172 (1966).